Kondo and charge fluctuation resistivity due to Anderson impurities in graphene

Sung-Po Chao and Vivek Aji
Department of Physics and Astronomy, University of California, Riverside, California 92521, USA
(Received 1 December 2010; revised manuscript received 11 February 2011; published 29 April 2011)

Motivated by experiments on ion-irradiated graphene, we compute the resistivity of graphene with dilute impurities. In the local moment regime we employ the perturbation theory up to third order in the exchange coupling to determine the behavior at high temperatures within the Kondo model. Resistivity due to charge fluctuations is obtained within the mean-field approach on the Anderson impurity model. Due to the linear spectrum of the graphene, the Kondo behavior is shown to depend on the gate voltage applied. The location of the impurity on the graphene sheet is an important variable determining its effect on the Kondo scale and resistivity. Our results show that for chemical potential near the node the charge fluctuations is responsible for the observed temperature dependence of resistivity, while away from the node the spin fluctuations take over. Quantitative agreement with experimental data is achieved if the energy of the impurity level varies linearly with the chemical potential.

DOI: 10.1103/PhysRevB.83.165449 PACS number(s): 72.80.Vp, 72.10.Fk

I. INTRODUCTION

A logarithmic upturn in the resistivity at low temperature has been observed in graphene with vacancies.[1] A fit to the temperature dependence of resistivity with conventional Kondo effect yields a large Kondo temperature (with $T_k \simeq 30 \sim 90$ K), which shows a nonmonotonic behavior with respect to the gate voltage.[1] The vacancies in the graphene sheets are induced by ion irradiation in ultrahigh vacuum and the magnetism in sputtered graphite has been experimentally observed.[2–6] Our goal is to study whether the Kondo effect alone in graphene can explain the experimental results in Ref. 1.

We start with the Anderson impurity model[7,8] to study the impurity effect on transport. In the local moment regime where the impurity occupation for a given spin $n_{d,s} \simeq 0.5$ we use the Schrieffer-Wolff transformation[9] to write down the Kondo model from the Anderson impurity Hamiltonian. Since we are interested in the resistivity due to impurity spin fluctuations, we study the Kondo model by a standard perturbation method. The perturbative approach fails at $T \simeq T_k$, with T_k representing the Kondo temperature but works for $T_k \ll T$. We compute the scattering rates in this weak-coupling regime. The scattering rates are determined via perturbative calculations of the T matrix.[10–12] The Kondo effect in the pseudogap system has been explored in the context of graphene as well as in that of a d-wave superconductor[13–20] via various different approaches such as numerical renormalization group (NRG) or the mean-field approach.[7,8] The advantage of our approach is the ability to determine high-temperature behavior of the scattering rate and resistivity accurately within a perturbation theory.

We assume a dilute concentration of impurities and ignore the spin-spin interactions, such as the Ruderman-Kittel-Kasuya-Yosida (RKKY) interaction. In graphene these interactions, in addition to being oscillatory with distance between impurities, depend on the sublattice on which the impurities are located.[21,22] For a chemical potential at the Dirac point our results are in agreement with the prediction of the existence of an intermediate coupling fixed point.[13–16] Near the node the exchange coupling J needs to be larger than a critical value J_c to have the Kondo effect. The dependence of T_k on the chemical potential is qualitatively different for $\mu \ll T_k$ and $\mu \gg T_k$. For impurities breaking the lattice symmetry, a power law in T divergence of the scattering rate is obtained for $\mu \ll T_k$, while a logarithmic divergence appears for $\mu \gg T_k$. For impurities preserving the lattice symmetry, a power law in T^3 divergence of the scattering rate is obtained for $\mu \ll T_k$, while a similar logarithmic divergence appears for $\mu \gg T_k$. For both cases the scaling of resistivity with a single Kondo temperature breaks down in the vicinity of the Dirac point. Our results for the Kondo temperature obtained within the T-matrix formalism is in agreement with the mean-field results for the development of the Kondo phase.[7,17] The resistivity obtained displays for different chemical potential dependences. For impurities breaking the lattice symmetry the resistivity decreases as the chemical potential increases, while for impurities preserving the lattice symmetry the resistivity increases as the chemical potential increases. For the same set of physical parameters the dominant source of resistivity is from impurities, which breaks the lattice symmetry.

We also explore the region near the empty orbital to the mixed valence one in the Anderson impurity model to find the resistivity due to charge fluctuations. From the NRG[14,15] the Kondo effect is suppressed as the critical exchange coupling $J_c \to \infty$ for a chemical potential close to the Dirac point. Thus we use the unrestricted Hatree-Fock method[23] on the Anderson impurity model to find the resistivity near the empty orbital regime. The resulting resistivity shows a similar dependence on the chemical potential as well as dominance from symmetry-breaking impurities as the resistivity obtained in the Kondo model. Near the node the Kondo scale, extracted from the logarithmic temperature dependence region on resistivity, yields a Kondo temperature comparable to the observations in the experiment in Ref. 1, while away from the Dirac point the extracted Kondo scale is higher than the experiment by one order of magnitude.

By combining the charge fluctuation effect for $\mu \simeq 0$ and the Kondo effect (spin fluctuations) for finite μ, we obtain a Kondo temperature dependence on μ that is qualitatively consistent with experimental results[1] with a gate voltage of less than 30 V. Our conclusion is that the observed experimental results, albeit fitted well by NRG for a conventional metal

Kondo model,[24] cannot be solely explained by Kondo screening in the entire range of chemical potentials. For a chemical potential near the node the charge fluctuations is responsible for the observed resistivity temperature dependence, while away from the node the spin fluctuations take over.

This paper is organized as following: We start with the Anderson impurity Hamiltonian to describe the dilute impurity physics in the graphene system. To study the local moment regime we use the Schrieffer-Wolff transformation to obtain the Kondo model from the Anderson Hamiltonian. In Sec. III we evaluate resistivity due to spin fluctuations, with different impurity locations, by perturbation computations on the Kondo model. In Sec. IV we compute the resistivity due to charge fluctuations when the impurity occupation is close to zero by using a mean-field approach on the Anderson model. In Sec. V we show the numerical results of temperature dependence of the resistivity with different symmetries and mechanisms. In Sec. VI we compare our results with the experiment in Ref. 1. The results are summarized in Sec. VII. Two appendixes contain derivations for the perturbative results in the Kondo model.

II. HAMILTONIAN

We start from a graphene Hamiltonian in the presence of dilute impurities described by the Anderson impurity Hamiltonian,[7]

$$\begin{aligned} H &= H_g + H_d + H_U + H_V, \\ H_g &= -t\sum_{k,s}\phi_k a^\dagger_{k,s} b_{k,s} + \text{H.c.} - \mu(a^\dagger_{k,s}a_{k,s} + b^\dagger_{k,s}b_{k,s}), \\ H_d &= \sum_s \epsilon_d d^\dagger_s d_s, \\ H_U &= U d^\dagger_s d_s d^\dagger_{-s} d_{-s}, \\ H_V &= \sum_{k,s}[V^*_{a,k}a^\dagger_{k,s} + V_{b,k}b^\dagger_{k,s}]d_s + \text{H.c.} \end{aligned} \tag{1}$$

H_g is the nearest hopping in the momentum space, with $t \simeq 2.7$ eV being the nearest-neighbor hopping strength. μ defines the Fermi level measured from the Dirac point. $a^\dagger_{k,s}$ and $b^\dagger_{k,s}$ are the particle creation operators on the a and b sublattices. $\phi_k = \sum_{i=1}^3 e^{i\vec{k}\cdot\vec{a}_i}$, with $\vec{a}_1 = a_0\vec{x}$, $\vec{a}_2 = a_0(-\vec{x}/2 + \sqrt{3}\vec{y}/2)$, and $\vec{a}_3 = a_0(-\vec{x}/2 - \sqrt{3}\vec{y}/2)$ being the nearest-neighbor lattice vector. $a_0 \simeq 1.42$ Å is the lattice constant. H_V describes the hybridization between the impurity level and graphene electrons with $V_{k,a/b} = \sum_{i=1}^3 V_{i,a/b}e^{i\vec{k}\cdot\vec{a}_i}$. H_U describes the Coulomb repulsion on the impurity level and H_d is the Hamiltonian describing the localized level of the d electron. We diagonalize H_g by defining $c^\dagger_{ks\pm} = [a^\dagger_{ks} \pm (\phi_k/|\phi_k|)b^\dagger_{ks}]$. In this basis the H_g term becomes

$$H_g = \sum_{ksn}(nt|\phi_k| - \mu)c^\dagger_{ksn}c_{ksn}, \tag{2}$$

with $n = \pm$ denoting the conduction and valence bands. The hybridization term H_V in this rotated basis is

$$H_V = V\sum_{n=\pm}\sum_{k,s}[\Theta_{kn}c^\dagger_{ksn}d_s + \text{H.c.}],$$

with $\Theta_{kn} = (V_{k,b} + nV^*_{k,a}\phi^*_k/|\phi_k|)/(\sqrt{2}V)$. Denote $\epsilon_{k,n} = nt|\phi_k| - \mu$ as the energy of the bands evaluated from the chemical potential μ and $\{k\} = (\vec{k}sn)$ as combinations of momentum, spin, and n the band index. The Anderson impurity Hamiltonian describing the impurity in the graphene can be written as

$$\begin{aligned} H = &\sum_{\{k\}}\epsilon_{kn}c^\dagger_{ksn}c_{ksn} + \sum_s \epsilon_d d^\dagger_s d_s + U d^\dagger_s d_s d^\dagger_{-s}d_{-s} \\ &+ V\sum_{\{k\}}[\Theta_{kn}c^\dagger_{ksn}d_s + \Theta^*_{kn}d^\dagger_s c_{ksn}]. \end{aligned} \tag{3}$$

To explore the local moment regime where impurity occupation for a given spin $n_{d,s} \simeq 0.5$, we perform a Schrieffer-Wolf transformation to project out the charge degree of freedom.[7] The exchange Hamiltonian or Kondo model obtained after this transformation with the additional term $H_{\text{int}} \propto \vec{S}_r \cdot \vec{S}_{r'}$ describing spin-spin interaction at different sites is given by $H = H_g + H_{\text{imp}} + H_{\text{int}}$, with

$$\begin{aligned} H_g &= \sum_{\{k\}}\epsilon_{kn}c^\dagger_{ksn}c_{ksn}, \\ H_{\text{imp}} &= \frac{1}{N}\sum_{\{k\},\{k'\}}\Theta^*_{kn}\Theta_{k'm}\left(K\delta_{s's} - \frac{J}{2}\vec{S}\cdot\vec{\sigma}_{s's}\right)c^\dagger_{k's'm}c_{ksn}, \\ H_{\text{int}} &= -\sum_{r,r'}W(r-r')\vec{S}_r\cdot\vec{S}_{r'} \end{aligned} \tag{4}$$

Here $J \simeq V^2[1/(\epsilon_d - \mu) - 1/(\epsilon_d + U - \mu)]$ and $K \simeq (V^2/2)[1/(\mu - \epsilon_d) + 1/(\mu - \epsilon_d - U)]$. The interaction between impurity spins H_{int} is added for the inclusion of the spin-spin interaction but is assumed to be small due to a small concentration of the impurities in this paper. Including this term would lead to a time-dependent impurity spin via $S(\tau) = e^{H_{\text{int}}\tau}Se^{-H_{\text{int}}\tau}$, with τ being the imaginary time.[10]

For impurities preserving the C_{3v} point group symmetry of the triangular sublattice in the graphene system, the factor $|\Theta_{kn}| \propto |\phi_k|$, while for impurities breaking the symmetry the factor $|\Theta_{kn}|$ is a constant. To evaluate the resistivity due to spin fluctuations we use Eq. (4) as the starting Hamiltonian. We use a perturbation expansion on the one-particle Green's function T matrix to compute the scattering rate and from the Boltzmann transport to obtain a linear response resistivity in both impurity breaking and preserving the lattice symmetry cases. We use a mean-field approach on the Anderson impurity model shown in Eq. (3) to obtain resistivity due to charge fluctuations in both symmetry breaking and preserving cases. The following two sections are the computation results for each of the cases mentioned above.

III. RESISTIVITY DUE TO IMPURITY SPIN FLUCTUATIONS

To study the resistivity due to spin fluctuations we start with the Kondo Hamiltonian shown in Eq. (4). We calculate

transport properties from the T matrix, which is related to the single-particle Green's function by[10]

$$G_{\{k'\},\{k\},\alpha',\alpha}(i\omega_1,i\omega_2) = G^0_{\{k'\},\{k\}}(i\omega_1) + G^0_{\{k'\},\{k'\}}(i\omega_1)T_{\{k'\},\{k\},\alpha',\alpha} \times (i\omega_1,i\omega_2)G^0_{\{k\},\{k\}}(i\omega_2), \quad (5)$$

where $G^0_{\{k'\},\{k\}}(i\omega_1) = \delta_{k',k}\delta_{s',s}\delta_{m,n}(i\omega_1 - \epsilon_{k,n})^{-1}$ and α, α' are impurity spin state indices. The formalism used is the generalization when one is interested in accounting for the dynamics of the spins.[10] When the dynamics of spins are trivial, $H_{\rm RKKY} = 0$, i.e., governed by the coupling to the conduction electron spin. The thermodynamic average is performed, as shown in Eqs. (9), (11), and (12) below, by replacing two spin correlation functions $\langle s(t)s(0)\rangle$ by $s(s+1)$. This expression is related to the time-dependent Green's function by

$$G_{\{k'\},\{k\},\alpha',\alpha}(i\omega_1,i\omega_2) = \int_0^\beta \int_0^\beta d\tau\, d\tau' e^{i(\omega_1\tau - \omega_2\tau')} G_{\{k'\},\{k\},\alpha',\alpha}(\tau,\tau'), \quad (6)$$

with $\omega = (2r+1)\pi T = (2r+1)\pi/\beta$ and r being integers (We put the Boltzmann constant $k_B = 1$ to simplify the notation.) Based on perturbation in $H_{\rm int}$ this time-dependent Green's function can be written as

$$G_{\{k'\},\{k\},\alpha',\alpha}(\tau,\tau') = -\langle Z\rangle^{-1}\sum_{n=0}^{\infty}\frac{(-1)^n}{n!}\int_0^\beta d\tau_1\cdots\int_0^\beta d\tau_n \sum_{q_1,q_1',\ldots,q_m,q_n'}\sum_{s_1,s_1',\ldots,s_n,s_n'}\sum_{n_1,m_1,\ldots,n_m,m_n} \times\left\{T_S\left[\Theta^*_{k_1',n_1}\Theta_{k_1',m_1}\left(K\delta_{s_1',s_1} - \frac{J}{2}\vec{S}(\tau_1)\cdot\vec{\sigma}_{s_1',s_1}\right)\cdots\Theta^*_{k_n',n_n}\Theta_{k_n',m_n}\left(K\delta_{s_n',s_n} - \frac{J}{2}\vec{S}(\tau_n)\cdot\vec{\sigma}_{s_n',s_n}\right)\right]\right\}_{\alpha',\alpha} \times\langle T_\tau(c_{k's'm}(\tau)\bar{c}_{ksn}(\tau')\bar{c}_{k_1's_1'm_1}(\tau_1)c_{k_1s_1n_1}(\tau_1)\cdots\bar{c}_{k_n's_n'm_n}(\tau_n)c_{k_ns_nn_n}(\tau_n)\rangle_{H_e}. \quad (7)$$

Here T_S and T_τ are the time ordering operators and $\langle Z\rangle$ is the S matrix. The first order in J and K is given by

$$T^{(1)}_{\{k'\},\{k\},\alpha',\alpha}(i\omega_1,i\omega_2) = \Theta^*_{kn}\Theta_{k'm}\left[\beta\delta_{\omega_1,\omega_2}K\delta_{s',s}\delta_{\alpha',\alpha} - \frac{J}{2}\sigma_{s's}S_{\alpha'\alpha}(i(\omega_1-\omega_2))\right]. \quad (8)$$

Here $S(i\omega') = \int_0^\beta d\tau\, e^{i\omega'\tau}S(\tau)$, with $\omega' = 2\pi r k_B T$. For $H_{\rm RKKY} = 0$ we can simplify the above expression by noting that $S(i\omega') = \beta S\delta_{\omega',0}$, and we get

$$T^{(1)}_{\{k'\},\{k\},\alpha',\alpha}(i\omega_1,i\omega_2) = \beta\delta_{\omega_1,\omega_2}T^{(1)}_{\{k'\},\{k\},\alpha',\alpha}(i\omega_1), \quad (9)$$

with $T^{(1)}_{\{k'\},\{k\},\alpha',\alpha}(i\omega_1) = \Theta^*_{kn}\Theta_{k'm}(K - \frac{J}{2}\sigma_{s's}S_{\alpha'\alpha})$. The general second-order result of the T matrix, with $f_{k,n} \equiv 1/(e^{\beta\epsilon_{k,n}}+1)$ and $F(z) \equiv N^{-1}\sum_{k,n}|\Theta_{kn}|^2(z-\epsilon_{k,n})^{-1}$, is expressed as

$$\begin{aligned}T^{(2)}_{\{k'\},\{k\},\alpha',\alpha}(i\omega_1,i\omega_2) &= \Theta^*_{kn}\Theta_{k'm}\{\beta\delta_{\omega_1,\omega_2}\delta_{\alpha',\alpha}K^2 - KJ\sigma_{s's}S_{\alpha'\alpha}(i\omega_1 - i\omega_2)\}F(i\omega_1)\\ &+\Theta^*_{kn}\Theta_{k'm}\left(\frac{J}{2}\right)^2 T\sum_{\omega_1'\omega_2'}(\sigma^{i_1}\sigma^{i_2})_{s's}\delta_{\omega_1'+\omega_2',\omega_1-\omega_2}\\ &\times\frac{1}{N}\sum_{q,l}|\Theta_{ql}|^2G^0_{q,l}(i\omega_1 - i\omega_1')\\ &\times\{S^{i_1}(i\omega_1')S^{i_2}(i\omega_2') - f_{q,l}[S^{i_1}(i\omega_1'),S^{i_2}(i\omega_2')]\}_{\alpha'\alpha}.\end{aligned} \quad (10)$$

To focus on the Kondo contribution to the scattering rate, we may set $K = 0$ and we set $H_{\rm int} = 0$ by assuming dilute impurities. For RKKY types of spin-spin interactions the interaction strength decays as $1/R^3$ for symmetry breaking or $1/R^7$ for the symmetry preserving case.[7] Thus for sufficient dilute impurities we may treat $H_{\rm int} = 0$. In this limit Eq. (10) is simplified to $T^{(2)}_{\{k'\},\{k\},\alpha',\alpha}(i\omega_1,i\omega_2) = \beta\delta_{\omega_1,\omega_2}T^{(2)}_{\{k'\},\{k\},\alpha',\alpha}(i\omega_1)$, with

$$T^{(2)}_{\{k'\},\{k\},\alpha',\alpha}(z) = \Theta^*_{kn}\Theta_{k'm}\left(\frac{J}{2}\right)^2\left[S(S+1)F(z)\delta_{s',s}\delta_{\alpha',\alpha} + \frac{1}{N}\sum_{q,l}\frac{|\Theta_{ql}|^2}{\epsilon_{q,l}-z}\tanh\left(\frac{\beta\epsilon_{q,l}}{2}\right)(S_{\alpha'\alpha}\cdot\sigma_{s's})\right]. \quad (11)$$

For noninteracting spins the third-order perturbation, after taking a trace over conduction electron spins and approximating the reduction of three-spin correlation functions to two-spin correlation functions,[10] is given by

$$T^{(3)}(z) = 2S(S+1)\left(\frac{J}{2}\right)^3\Theta^*_{kn}\Theta_{k'm}\frac{1}{N^2} \times\sum_{q_1,n_1}\left[\frac{|\Theta_{q_1n_1}|^2}{z-\epsilon_{q_1,n_1}}\sum_{q_2,n_2}\frac{|\Theta_{q_2n_2}|^2\tanh\left(\frac{\beta\epsilon_{q_2,n_2}}{2}\right)}{\epsilon_{q_1,n_1}-\epsilon_{q_2,n_2}}\right]. \quad (12)$$

From Eqs. (11) and (12) we may define a general function $R(z)$ which we need to evaluate in computing the T-matrix,

$$R(z) = \frac{1}{N}\sum_{q,n}\frac{|\Theta_{qn}|^2}{\epsilon_{q,n}-z}\tanh\left(\frac{\beta\epsilon_{q,n}}{2}\right). \quad (13)$$

By using $\epsilon_{q,n} = nt|\phi_q| - \mu \simeq n\frac{3ta_0}{2}|q| - \mu = n|\epsilon| - \mu$ we may write the continuous form of Eq. (13) as

$$R(z) = \frac{8}{9\pi t^2}\int_{-\Lambda}^{\Lambda} d\epsilon|\epsilon|\frac{|\Theta_\epsilon|^2}{\epsilon-(z+\mu)}\tanh\left(\frac{\beta(\epsilon-\mu)}{2}\right), \tag{14}$$

where Λ is the linear spectrum cutoff. In the following we will separate the discussions into two cases:[7] One with impurity interactions breaking the C_{3v} lattice symmetry, in which $|\Theta_{kn}|^2 = \frac{1}{2}$, and we denote $R(z) = R_{\rm SB}(z)$ in this case; another with impurity interactions preserving the symmetry, in which $|\Theta_{kn}|^2 = \frac{9|k|^2a_0^2}{8} = \frac{|\epsilon|^2}{2t^2}$, and we denote $R(z) = R_{\rm SP}(z)$ in this case.

A. C_{3v} symmetry breaking impurities

For the case of symmetry breaking, the cutoff scheme we choose for a linear density of states (DOS) with a cutoff Λ is multiplying the argument of the right-hand side of Eq. (14) by $\frac{\Lambda^2}{\epsilon^2+\Lambda^2}$ and extending the integration limit from $\pm\Lambda$ to $\pm\infty$. The resulting $R_{\rm SB}(z)$, with details shown in Appendix A, is

$$\begin{aligned} R_{\rm SB}(z) = \frac{4}{9\pi t^2}\Bigg\{&\frac{\Lambda}{\pi}\Bigg[P\int_0^\infty \frac{x\,dx}{x-\Lambda}F(x,\mu,z) \\ &-\int_0^\infty \frac{x\,dx}{x+\Lambda}F(x,\mu,z)\Bigg] \\ &-\psi\left(\frac{1}{2}-i\frac{\beta z}{2\pi}\right)\frac{2\Lambda^2(z+\mu)}{(z+\mu)^2+\Lambda^2}\Bigg\}. \end{aligned} \tag{15}$$

Here $F(x,\mu,z)$ is defined as

$$F(x,\mu,z) = \frac{\psi\left(\frac{1}{2}+i\frac{\beta\mu}{2\pi}+\frac{\beta x}{2\pi}\right)}{x+i(\mu+z)} + \frac{\psi\left(\frac{1}{2}-i\frac{\beta\mu}{2\pi}+\frac{\beta x}{2\pi}\right)}{x-i(\mu+z)}.$$

and $\psi(z)$ is the digamma function. Analytic forms can be obtained in two asymptotic limits by using the asymptotic forms of the digamma function. For $\beta\mu \ll 2\pi$ we have

$$\begin{aligned} R_{\rm SB}(z) \simeq \frac{4}{9\pi t^2}\Bigg[&\pi\Lambda + \frac{4\gamma+4\ln(2)-4-3\zeta(2)}{\beta} \\ &-\frac{(4\gamma-2\zeta(2)+8)(z+\mu)}{\pi}\tan^{-1}\left(\frac{\pi}{\beta(z+\mu)}\right) \\ &+\frac{\beta z(z+\mu)}{2}\ln\left[1+\left(\frac{\pi}{\beta(z+\mu)}\right)^2\right] \\ &-\frac{2\Lambda^2(z+\mu)}{(z+\mu)^2+\Lambda^2}\psi\left(\frac{1}{2}-i\frac{\beta z}{2\pi}\right)\Bigg], \end{aligned} \tag{16}$$

where $\gamma \simeq 0.577$ is the Euler constant and $\zeta(2) = \pi^2/6$ is the Riemann zeta function evaluated at 2. In the limit $\beta\mu \gg 2\pi$ we get

$$\begin{aligned} R_{\rm SB}(z) \simeq \frac{4}{9\pi t^2}\Bigg\{&\frac{4}{\pi}\ln\left(\frac{\beta|\mu|}{2\pi}\right)(z+\mu)\tan^{-1}\left(\frac{|\mu|}{z+\mu}\right) \\ &+\pi\Lambda + \frac{4|\mu|}{\pi}\left[\frac{\pi}{2}-\tan^{-1}\left(\frac{|\mu|}{z+\mu}\right)-1\right] \\ &-|z+\mu|\ln\left(1+\frac{\mu^2}{\mu^2+z^2}\right) \\ &-\frac{2\Lambda^2(z+\mu)}{(z+\mu)^2+\Lambda^2}\psi\left(\frac{1}{2}-i\frac{\beta z}{2\pi}\right)\Bigg\}. \end{aligned} \tag{17}$$

In Eqs. (16) and (17) we have assumed $0 \leqslant z \leqslant \mu$. Using the Boltzmann equation with a relaxation time hypothesis[25] and noticing that the honeycomb symmetry is broken by the impurity, we find the scattering rate is related to the T matrix by

$$\begin{aligned} &\frac{1}{\tau_{\rm SB}(\epsilon_{k,n})} \\ &= \frac{\pi n_I}{\hbar}\int \delta(\epsilon_{k,n}-\epsilon_{k',m})|T_{k,k'}|^2(1-\cos\theta_{k,k'})\frac{d\vec{k'}}{(2\pi)^2} \\ &\quad+\frac{\pi n_I}{\hbar}\int \delta(\epsilon_{k,n}-\epsilon_{k',m})|T_{k,k'}|^2(1-\cos\theta_{k,k'})\frac{d\vec{k'}}{(2\pi)^2} \\ &= -\frac{2n_I}{\hbar}{\rm Im}[T_{k,k}(\epsilon_{k,n})]. \end{aligned} \tag{18}$$

The second line of Eq. (18) represents the scattering process related to different Dirac points in the Brillouin zone, and the third line is the scattering event within the same Dirac cone. We have used the fact that ${\rm Im}[T_{k,k}(\epsilon^+)] = -\pi\sum_{k'}|T_{k,k'}(\epsilon^+)|^2\delta(\epsilon-\epsilon_{k'})$ and $|T_{k,k'}(\epsilon^+)|^2$ is independent of angle $\theta_{k,k'}$ between momenta k and k' in the symmetry breaking case in the above equation. The scattering rate, $\tau_{\rm SB}^{-1}(\omega)$ with $\tau_{\rm SB}(\omega)$ being the relaxation time, to third order is

$$\begin{aligned} \hbar\tau_{\rm SB}^{-1}(\omega) = 4n_I S(S+1)\Bigg[&\left(\frac{2}{9t^2}\right)\left(\frac{J}{2}\right)^2|\omega+\mu| \\ &-2\left(\frac{2}{9t^2}\right)\left(\frac{J}{2}\right)^3|\omega+\mu|{\rm Re}[R(\omega)]\Bigg]. \end{aligned} \tag{19}$$

The Kondo effect is reflected in the divergence of the relaxation time in the parquet approximation. This involves treating the cubic term as the first in an infinite series, which is summed to give

$$\hbar\tau_{\rm SB}^{-1}(\omega) = 4n_I S(S+1)\left(\frac{2}{9t^2}\right)\left(\frac{J}{2}\right)^2\frac{|\omega+\mu|}{1+J\,{\rm Re}[R(\omega)]}. \tag{20}$$

We are mainly interested in the dc response so we shall study the relaxation time when $\omega \to 0$. Figure 1 shows the function $R_{\rm SB}(0)$ plotted as a function of temperature for different chemical potentials. We define the Kondo temperature as the temperature when the relaxation time diverges when $\omega \to 0$. For the case $\beta\mu \ll 2\pi$ the singularities from $1 + J\,{\rm Re}[R(0)] \simeq 0$ can be expressed, by using Eq. (16), as

$$\begin{aligned} &\frac{4J}{9\pi t^2}\left[\pi\Lambda + \frac{4\gamma+4\ln(2)-4-3\zeta(2)}{\beta_k}\right] \simeq -1 \\ &\to T_k = -\frac{\pi\Lambda}{4\gamma+4\ln(2)-4-3\zeta(2)}\left(1-\frac{J_c}{J}\right), \end{aligned} \tag{21}$$

where $J_c = -9t^2/4\Lambda$ and $\beta_k = 1/T_k$. Thus for chemical potential $\mu \ll T$ we have no Kondo effect if $|J| < |J_c|$. As one increases the chemical potential we may include the linear

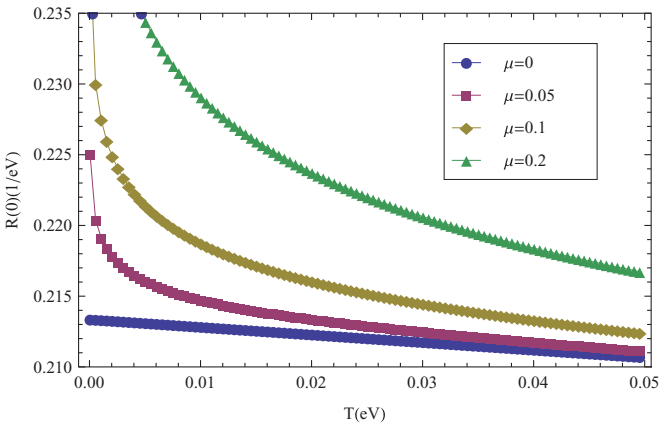

FIG. 1. (Color online) The function $R_{\rm SB}(0)$ plotted as a function of temperature $k_B T$ in the unit of eV. Energy cutoff $\Lambda = 3.5$ eV and $t = 2.7$ eV.

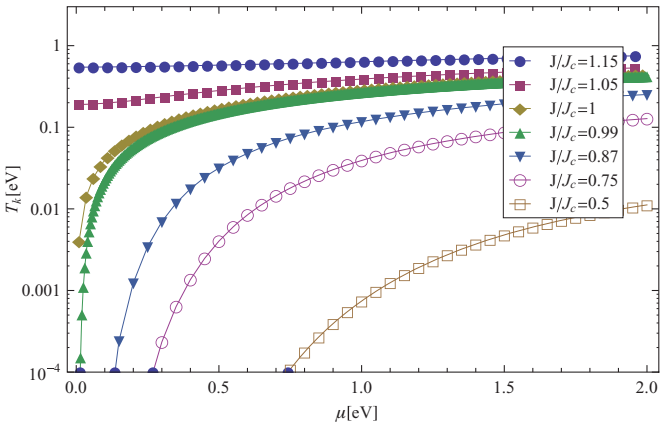

FIG. 2. (Color online) The Kondo temperature as a function of chemical potential for various values of J. Energy cutoff $\Lambda = 3.5$ eV and $t = 2.7$ eV gives $|J_c| \simeq 4.68$ eV.

order of μ in Eq. (16) and obtain the expression for the Kondo temperature as

$$T_k = -\frac{\pi\Lambda\left(1-\frac{J_c}{J}\right)+[4\ln(2)+\zeta(2)-4]\mu}{4\gamma+4\ln(2)-4-3\zeta(2)}, \qquad (22)$$

where we have used $\tan^{-1}(\frac{\pi}{\beta(z+\mu)}) \to \frac{\pi}{2}$ and $\psi(\frac{1}{2}) = -\gamma - 2\ln(2)$. Thus the Kondo temperature increases with increasing chemical potential.

In the opposite limit where $\beta\mu \gg 2\pi$, we use Eq. (17) to obtain the Kondo temperature as

$$T_k = c_1 \mu \exp\left[\frac{\pi\Lambda}{\mu}\left(1-\frac{J_c}{J}\right)\right], \qquad (23)$$

where $c_1 = \exp[\gamma + \ln(2) - 1 - 4/\pi]/2\pi \simeq 0.058$. Equation (23) can be expressed as $T_k \propto \exp[(J - J_c)/(\rho_g J)]$, with $\rho_g \propto \mu$ the electron DOS of graphene. Compared with the Kondo temperature in conventional metal $T_k \propto \exp(1/\rho_g J)$, there exists acritical value of exchange coupling for the Kondo effect to be realized in this two-dimensional pseudogap system. Figure 2 shows the Kondo temperature as a function of the chemical potential for various values of J. For J/J_c smaller than 0.87, the Kondo temperature is smaller than the chemical potential for the range shown. In this regime T_k is given by Eq. (23) and is exponentially smaller than the energy scale set by the chemical potential. As J/J_c approaches one from below, the Kondo temperature grows faster than the chemical potential. As $T_k(\mu) \simeq \mu/2\pi$ the exponential behavior crosses over to the linear dependence shown in Eq. (22).

Given the relaxation time we obtain the linear response conductivity as

$$\sigma^s_{\rm SB}(T) = -\frac{2e^2}{3}\sum_n \int v_F^2 \tau_{\rm SB}(\epsilon_{k,n})\frac{\partial f}{\partial \epsilon_{k,n}}\frac{d\vec{k}}{(2\pi)^2}$$
$$= -\frac{2e^2}{3}\frac{4v_F^2}{9\pi a_0^2 t^2}\int_{-\infty}^{\infty} d\epsilon|\epsilon|\tau_{\rm SB}(\epsilon-\mu)\frac{\partial f}{\partial \epsilon}. \qquad (24)$$

For a small chemical potential or $\beta\mu \ll 2\pi$ we use Eqs. (16), (20), and (22) and approximate $\int g(\epsilon)(-\partial f/\partial\epsilon) \simeq \int_{\mu-T}^{\mu+T} g(\epsilon)/(2T)$ since the dominant contribution is for energies close to μ. We get the resistivity at a low chemical potential as

$$\rho^s_{\rm SB}(T) \simeq \frac{3}{2e^2}\frac{\pi S(S+1)a_0^2 n_I}{\hbar v_F^2}\left(\frac{J}{2}\right)^2\frac{9\pi t^2}{2J}\left(\frac{1}{r(T,\mu)}\right)$$
$$\simeq \frac{3\pi n_I S(S+1)}{4}\left(\frac{J}{2}\right)\frac{h}{e^2}\left(\frac{1}{r(T,\mu)}\right), \qquad (25)$$

with

$$r(T,\mu) = [4\gamma + 4\ln(2) - 4 - 3\zeta(2)](T - T_k)$$
$$-\left[2\gamma - \zeta(2) + 4 - 2\psi\left(\frac{1}{2}\right)\right]\frac{(T-\mu)^2}{2T}.$$

For temperature $\mu/2\pi < T < \mu$ but higher than T_k, the same approximation scheme gives

$$\rho^s_{\rm SB}(T) \simeq \frac{3\pi n_I S(S+1)}{4}\left(\frac{J}{2}\right)\frac{h}{e^2}\left(\frac{1}{r(T,\mu)}\right).$$
$$r(T,\mu) = [4\gamma + 4\ln(2) - 4 - 3\zeta(2)](T - T_k). \qquad (26)$$

Thus we see that for $T > \mu$ the Kondo contribution to resistance is not determined by a single scale T_k. For temperature range between $\mu/2\pi < T < \mu$ the scaling of the resistivity goes as $1/(T - T_k)$. This power-law behavior indicates that at a sufficiently low chemical potential the magnetic impurities are not completely quenched while a logarithmic behavior is expected in the conventional metal case.

For large μ or $\beta\mu \gg 2\pi$, a Kondo effect similar to magnetic impurities in the conventional metals is obtained. For a large chemical potential we approximate $\partial f/\partial\epsilon \simeq -\delta(\epsilon - \mu)$. Under this approximation the resistivity $\rho^s_{\rm SB}(T) = \frac{1}{\sigma^s_{\rm SB}(T)}$ is given by

$$\rho^s_{\rm SB}(T) \simeq \frac{3}{2e^2}\frac{\pi S(S+1)a_0^2 n_I}{\hbar v_F^2}\frac{\left(\frac{J}{2}\right)^2}{1 + J\,{\rm Re}[R_{\rm SB}(0)]}. \qquad (27)$$

Using Eq. (17) for ${\rm Re}[R_{\rm SB}(0)]$ with $T > T_k$ we get

$$\rho^s_{\rm SB}(T) \simeq \frac{3}{2e^2}\frac{\pi S(S+1)a_0^2 n_I}{\hbar v_F^2}\left(\frac{J}{2}\right)^2\frac{9\pi t^2}{2J\mu}\left(\ln\left[\frac{T_k}{T}\right]\right)^{-1}$$
$$\simeq \frac{3\pi n_I S(S+1)}{4}\left(\frac{J}{2\mu}\right)\frac{h}{e^2}\left(\ln\left[\frac{T_k}{T}\right]\right)^{-1}. \qquad (28)$$

B. C_{3v} symmetry preserving impurities

For the case of impurities preserving the symmetry of a honeycomb lattice, the cutoff scheme we choose for a linear DOS with a cutoff Λ is to multiply the argument of the right-hand side of Eq. (14) by $\Lambda^4/(\epsilon^4+\Lambda^4)$ and extend the integration limit from $\pm\Lambda$ to $\pm\infty$. The resulting $R_{\rm SP}(z)$, with details shown in Appendix B, is

$$\begin{aligned} R_{\rm SP}(z) = \frac{4}{9\pi t^4}\Bigg\{ & \frac{2\Lambda^4}{\pi}\int_0^\infty dx \frac{x^3}{x^4+\Lambda^4}F(x,\mu,z) \\ & -2\frac{(z+\mu)^3\Lambda^4}{\Lambda^4+(z+\mu)^4}\psi\left(\frac{1}{2}-i\frac{\beta z}{2\pi}\right) \\ & +\mathrm{Re}\Bigg[\frac{\Lambda^4\psi\left(\frac{1}{2}+i\frac{\beta\mu}{2\pi}-i\frac{\beta\Lambda}{2\pi}e^{i\frac{3\pi}{4}}\right)}{\Lambda e^{i\frac{3\pi}{4}}-(z+\mu)} \\ & -\frac{\Lambda^4\psi\left(\frac{1}{2}-i\frac{\beta\mu}{2\pi}-i\frac{\beta\Lambda}{2\pi}e^{i\frac{\pi}{4}}\right)}{\Lambda e^{i\frac{\pi}{4}}-(z+\mu)}\Bigg]\Bigg\}. \end{aligned} \tag{29}$$

Analytic forms of $R_{\rm SP}(z)$ are obtained by taking the asymptotic behavior of the digamma function in the following two limits: $\beta\mu/2\pi \ll 1$ and $\beta\mu/2\pi \gg 1$. For $\beta\mu/2\pi \ll 1$ we have

$$\begin{aligned} R_{\rm SP}(z) \simeq \frac{4\Lambda^3}{9\pi t^4}\Bigg\{ & \frac{\pi}{\sqrt{2}}+\frac{\left[\pi-4\ln\left(\frac{2\pi}{\beta\Lambda}\right)\right]\frac{z\mu}{\Lambda^2}}{\sqrt{2}} \\ & +\left(1-\frac{\left[4+8\ln\left(\frac{z}{\Lambda}\right)\right]z}{\pi\Lambda}\right)\frac{\pi}{\beta\Lambda} \\ & +\frac{\sqrt{2}}{3}\left(1+\frac{2z\mu}{\Lambda^2}\right)\left(\frac{\pi}{\beta\Lambda}\right)^2 \\ & +\left(\frac{4[1+2\ln(2)]}{9\pi}+\frac{\mu}{2\pi z}\right)\left(\frac{\pi}{\beta\Lambda}\right)^3 \\ & +O\left[\left(\frac{\mu}{\Lambda}\right)^2,\left(\frac{z}{\Lambda}\right)^2\right]\Bigg\}. \end{aligned} \tag{30}$$

For the opposite limit $\beta\mu/2\pi \gg 1$ we have

$$\begin{aligned} R_{\rm SP}(z) \simeq \frac{4\Lambda^3}{9\pi t^4}\Bigg\{ & \frac{\pi}{\sqrt{2}}+\frac{2\pi}{\beta\Lambda} \\ & +\frac{(z+\mu)}{\pi\Lambda}\Bigg[\frac{2\mu}{\Lambda}-(2+\pi)\frac{\mu^2}{\Lambda^2} \\ & +2\left(1+\frac{\mu^2}{\Lambda^2}\right)\tan^{-1}\left(\frac{\mu}{\Lambda}\right)\Bigg] \\ & +\frac{z\mu}{\sqrt{2}\Lambda^2}\left[\pi-2-4\ln\left(\frac{\pi}{\beta\Lambda}\right)\right] \\ & +\frac{4}{\Lambda^3\pi}\Bigg[-\mu(z+\mu)^2+(z+\mu)^3\tan^{-1}\left(\frac{\mu}{z+\mu}\right) \\ & +\frac{\mu^3}{3}\Bigg]\ln\left(\frac{\beta\mu}{2\pi}\right)+\frac{\mu^2(\mu+z)}{\Lambda^3} \\ & +\frac{(\mu+z)^3}{\Lambda^3}\ln\left(\frac{(\mu+z)^2}{\mu^2+(\mu+z)^2}\right)\Bigg\}. \end{aligned} \tag{31}$$

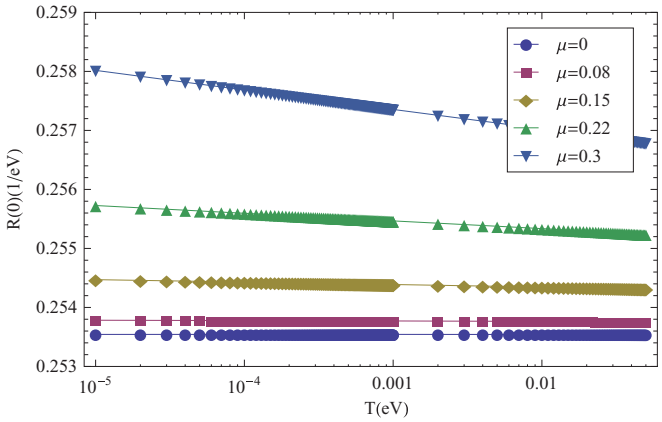

FIG. 3. (Color online) The function $R_{\rm SP}(0)$ plotted as a function of temperature k_BT in units of eV. Energy cutoff $\Lambda = 3.5$ eV and $t = 2.7$ eV. Compared with Fig. 2, $R_{\rm SP}(0)$ shows more temperature variations when $T \to 0$, indicating the Kondo effect can only be observed on a lower temperature as compared with the symmetry breaking case.

Similar to Eqs. (16) and (17) we have assumed $0 \leqslant z \leqslant \mu$. Using Eq. (18), but with the appropriate relaxation times determined in this section, we compute the resistance. For this case $\mathrm{Im}[T_{k,k}(\epsilon^+)] = -\pi\sum_{k'}|T_{k,k'}(\epsilon^+)|^2\delta(\epsilon-\epsilon_{k'})$ and $|T_{k,k'}(\epsilon^+)|^2$ is independent of angle $\theta_{k,k'}$ between momenta k and k' since $|T_{k,k'}(\epsilon^+)|^2 \propto |k|^2|k'|^2$. The scattering rate to third order is

$$\begin{aligned} \hbar\tau_{\rm SP}^{-1}(\omega) = 4n_I S(S+1)\Bigg[& \left(\frac{2}{9t^4}\right)\left(\frac{J}{2}\right)^2|\omega+\mu|^3 \\ & -2\left(\frac{2}{9t^4}\right)\left(\frac{J}{2}\right)^3|\omega+\mu|^3\,\mathrm{Re}[R_{\rm SP}(\omega)]\Bigg]. \end{aligned} \tag{32}$$

The expression for the relaxation time $\tau_{\rm SP}$ within the same approach as the previous section is

$$\hbar\tau_{\rm SP}^{-1}(\omega) = 4n_I S(S+1)\left(\frac{2}{9t^4}\right)\left(\frac{J}{2}\right)^2\frac{|\omega+\mu|^3}{1+J\,\mathrm{Re}[R_{\rm SP}(\omega)]}. \tag{33}$$

The dc conductivity is related to the relaxation time with $\omega \to 0$. Figure 3 shows the function $R_{\rm SP}(0)$ plotted as a function of temperature for different chemical potentials. $R_{\rm SP}(0)$ shows small variations with temperature except when the temperature is close to zero, where exponential growth with decreasing temperature is observed. For the case $\beta\mu \ll 2\pi$ the singularities from $1 + J\,\mathrm{Re}[R_{\rm SP}(0)] \simeq 0$ can be expressed, by using Eq. (30), as

$$\begin{aligned} & \frac{4J}{9\pi t^4}\left[\frac{\pi\Lambda^3}{\sqrt{2}}-\frac{1}{2\pi}\left(\frac{\pi}{\beta_k}\right)^3\right] \simeq -1 \\ & \to T_k \simeq \left(\frac{\sqrt{2}\Lambda^3}{\pi}\right)^{\frac{1}{3}}\left(1-\frac{J_c}{J}\right)^{\frac{1}{3}}. \end{aligned} \tag{34}$$

In the above we have used the leading-order correction as $(1/\beta)^3$ since its prefactor is μ/z, which diverges as we take $z \to 0$. Higher-order expansion in μ/z shows it as a sum of an infinite series in powers of $(-\mu/z)^n$, with n being some integer. Thus the infinite sum gives a factor of -1.

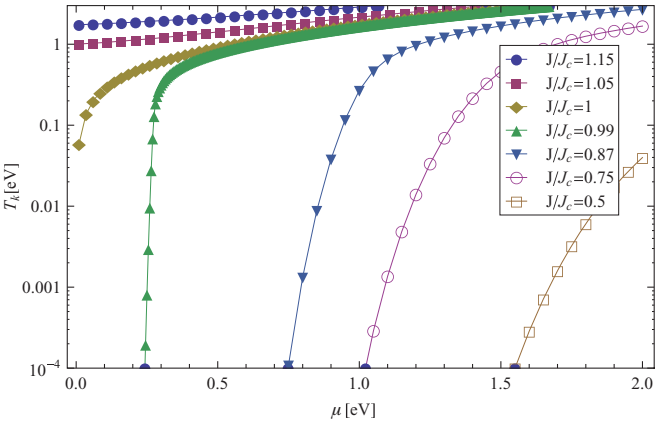

FIG. 4. (Color online) The Kondo temperature as a function of chemical potential for various values of J. Energy cutoff $\Lambda = 3.5$ eV and $t = 2.7$ eV gives $|J_c| = \frac{9\sqrt{2}t^4}{4\Lambda^3} \simeq 3.94$ eV for the symmetry preserving case.

In the opposite limit where $\beta\mu \gg 2\pi$ we use Eq. (31),

$$\frac{4J}{9\pi t^4}\left[\frac{\pi\Lambda^3}{\sqrt{2}} + \frac{4}{\pi}\Lambda\mu^2 + \left(1 - \frac{8}{3\pi}\right)\mu^3 \ln\left(\frac{\beta_k\mu}{2\pi}\right)\right] \simeq -1$$

$$\rightarrow\ T_k \simeq \frac{\mu}{2\pi}\exp\left[c_2\left(\frac{\Lambda}{\mu}\right)^3\left(1 - \frac{J_c}{J}\right) + c_3\frac{\Lambda}{\mu}\right], \qquad (35)$$

where $c_2 = \frac{3\pi^2}{\sqrt{2}(3\pi-8)} \simeq 14.69$, and $c_3 = \frac{\pi^2}{4\sqrt{2}} \simeq 1.74$. Thus for both cases we obtain results similar to mean-field results obtained in Ref. 7.

Figure 4 shows the Kondo temperature as a function of chemical potential for various exchange coupling strengths J. For J/J_c smaller than 0.75 the Kondo temperature is always smaller than the chemical potential for the range shown. J/J_c approaches one from below and for $T_k \simeq \mu/2\pi$ the exponential dependence on μ crosses over to a power law.

Given the relaxation time we obtain the linear response conductivity as

$$\sigma^s_{\rm SP}(T) = -\frac{2e^2}{3}\sum_n \int v_F^2 \tau_{\rm SP}(\epsilon_{k,n})\frac{\partial f}{\partial \epsilon_{k,n}}\frac{d\vec{k}}{(2\pi)^2}$$

$$= -\frac{2e^2}{3}\frac{4v_F^2}{9\pi a_0^2 t^2}\int_{-\infty}^{\infty} d\epsilon |\epsilon| \tau_{\rm SP}(\epsilon-\mu)\frac{\partial f}{\partial \epsilon}. \qquad (36)$$

For $\beta\mu \ll 2\pi$, $T > \mu$, and $T > T_k$ we use Eqs. (30) and (34) and again approximate $\int g(\epsilon)(-\partial f/\partial\epsilon) \simeq \int_{\mu-T}^{\mu+T} g(\epsilon)/(2T)$. The conductivity for $0 < \mu < T$ has no analytic form as the integral in Eq. (36) involves $\int_{\mu-T}^{\mu+T} d\epsilon/|\epsilon|^2$, which diverges as $\mu < T$. This vanishing resistivity for $\mu < T$ for impurities preserving the lattice symmetry is due to the fact that the scattering rate goes to zero faster than the chemical potential at the node. For C_{3v} symmetry preserving impurities the scattering rate goes as the third power of energy while the DOS is linear in energy. The vanishing resistivity is true even without the box approximation for the energy integral. Thus the contribution to scattering near the node is dominated by other sources of scattering as compared to exchange scattering of impurities that preserve the lattice symmetry.

For $\beta\mu \ll 2\pi$, $\mu/2\pi < T < \mu$, and $T > T_k$ we use Eqs. (30) and (34) and use the same approximation scheme as above, and we obtain the resistivity as

$$\rho^s_{\rm SP}(T) \simeq \frac{3}{2\pi}\frac{h}{e^2} n_I S(S+1) J \left(\frac{\mu^2 - T^2}{T_k^3 - T^3}\right). \qquad (37)$$

Thus even for larger chemical potentials the resistivity does not scale solely with the Kondo temperature. The behavior for $T < \mu$ goes as $\mu^2/(T^3 - T_k^3)$.

For large chemical potentials or $\beta\mu \gg 1$ we approximate $-\partial f/\partial\epsilon \simeq \delta(\epsilon - \mu)$. Combining with Eqs. (31) and (35) we get

$$\rho^s_{\rm SP}(T) \simeq \frac{9\pi^2}{(8\pi - 8)} n_I S(S+1)\frac{h}{e^2}\frac{J}{\mu}\left(\ln\left[\frac{T_k}{T}\right]\right)^{-1}. \qquad (38)$$

Thus at large chemical potentials the Kondo contribution to resistivity is similar in form to the magnetic impurities in a conventional metal.

IV. RESISTIVITY DUE TO IMPURITY CHARGE FLUCTUATIONS

From $|J| \simeq \frac{V^2|U|}{|(\epsilon_d-\mu)(\epsilon_d+U-\mu)|} \simeq V^2/|\mu - \epsilon_d|$, for a large Coulomb repulsion U, it follows that to obtain $|J| \geqslant |J_c|$ the impurity level ϵ_d must be close to the Fermi surface μ. Since the DOS in the graphene is proportional to the energy scale away from this Fermi surface, or $\rho_g(\epsilon) \propto |\epsilon|$ with $\rho_g(\epsilon)$ denoting the graphene DOS, the phase space for charge fluctuation is very small and the local moment region is large compared with the case of the magnetic impurities in a conventional metal.[7] However, it is still likely to have an impurity level close to μ which is not in the local moment region.[8] Thus it is worthwhile to estimate the resistivity contribution from impurity charge fluctuations.

We use a mean-field approach on the Anderson impurity model shown in Eq. (3) and rewrite $H_U \rightarrow \sum_s U n_{-s} d_s^\dagger d_s - U n_\uparrow n_\downarrow$, with $n_s = \langle d_s^\dagger d_s\rangle$ determined self-consistently, to obtain the impurity Green's function. From the imaginary part of this Green's function we obtain a temperature dependence of the linear response resistivity by assuming Boltzmann transport. Under this mean-field approach we obtain the retarded impurity Green's function as[8]

$$G^R_{dd,s}(\omega) = \frac{1}{\omega - \epsilon_d - U n_{-s} - \Sigma^R_{dd,s}(\omega) + i0^+}. \qquad (39)$$

The self-energy part $\Sigma^R_{dd,s}(\omega)$ is given by

$$\Sigma^R_{dd,s}(\omega) = \frac{V^2}{N}\sum_{\vec{q},n} |\Theta_{\vec{q},n}|^2 G^{0R}_{cc,s}(\vec{q},\omega)$$

$$= \frac{V^2}{N}\sum_{\vec{q}} \frac{|\Theta_q|^2(\omega+\mu)}{(\omega+\mu)^2 - v_F^2|q|^2 + i0^+{\rm sign}(\omega+\mu)}. \qquad (40)$$

In the above we have used $|\Theta_{\vec{q},n}| = |\Theta_q|^2$. $|\Theta_q|^2 = 1/2$ for the symmetry breaking case and $|\Theta_q|^2 = 9|q|^2 a_0^2/8$ for the symmetry preserving case. We take the principal part of $\Sigma^R_{dd,s}(\omega)$ between $(-\Lambda, \Lambda)$, with Λ being the linear spectrum cutoff. In the nonmagnetic mixed valence regime in which

we are interested in, $0 < n_s = n_{-s} < 1/2$. The impurity occupation n_s is given by

$$n_s = \int_{-\Lambda}^{\mu} d\omega \frac{-1}{\pi} \mathrm{Im}\big[G^R_{dd,s}(\omega)\big]. \tag{41}$$

By using Eqs. (39) and (40) we find the relation between ϵ_d and n_s by solving self-consistent conditions numerically.

A. C_{3v} symmetry breaking impurities

For impurities breaking the symmetry the self-energy $\Sigma^R_{dd,s}(\omega)$ obtained from Eq. (40) is given by

$$\Sigma^R_{dd,s}(\omega) = -\frac{2V^2}{9\pi t^2}\Bigg[(\omega+\mu)\ln \times \left(\frac{|(\omega+\mu)^2-\Lambda^2|}{(\omega+\mu)^2}\right) + i\pi|\omega+\mu|\Bigg].$$

Since $T_{k,k}(\omega) = \sum_s V^2|\Theta_k|^2 G^R_{dd,s}(\omega)$ we use Eqs. (18) and (24) to obtain the impurity conductivity, denoted as $\sigma^c_{\mathrm{SB}}(T)$. The resistivity $\rho^c_{\mathrm{SB}}(T) = 1/\sigma^c_{\mathrm{SB}}(T)$. We are mainly interested in the leading-order temperature dependence of the resistivity contributed by the charge fluctuation in the Anderson impurity model. Thus we use the same approximation $-\int g(\epsilon)\partial f/\partial\epsilon \simeq \int_{\mu-T}^{\mu+T} g(\epsilon)/2T$ in Eq. (24) to extract the leading order in temperature dependence. The resistivity obtained for $0 \simeq \mu < T$ is

$$\rho^c_{\mathrm{SB}}(T) \simeq \frac{9n_I V^4}{t^2}\frac{h}{e^2}\frac{1}{r(\mu,T)},$$

$$r(\mu,T) = 3T^2\alpha\ln\left(\frac{\Lambda^2-\tilde{\epsilon}_d^2}{T^2}\right)\left[3\alpha\ln\left(\frac{\Lambda^2-\tilde{\epsilon}_d^2}{T^2}\right)+4\alpha-6\right] + T^2[\alpha((8+9\pi^2)\alpha-12)+9] + 27(\tilde{\epsilon}_d+\mu)^2. \tag{42}$$

Here $\alpha \equiv \frac{-2V^2}{9\pi t^2}$ and $\tilde{\epsilon}_d \equiv \epsilon_d + Un_{-s}$. An analytic result of resistivity for $T \leqslant \mu$ can also be obtained but the expressions are cumbersome and we defer a numerical analysis to Sec. V. From Eq. (41) we find the nonmagnetic region[8] by demanding $n_s = n_{-s}$ when $\epsilon_d \simeq \mu$. Within this charge fluctuation regime ($0 \leqslant n_s \ll 0.5$) we study the temperature variation of resistivity at a given μ and Coulomb repulsion U.

B. C_{3v} symmetry preserving impurities

For impurities preserving the honeycomb lattice symmetry, the self-energy $\Sigma^R_{dd,s}(\omega)$ is given by

$$\Sigma^R_{dd,s}(\omega) = -\frac{2V^2}{9\pi t^4}\left[(\omega+\mu)^3 P\int_0^{\frac{\Lambda^2}{(\omega+\mu)^2}}\frac{x\,dx}{x-1} + i\pi|\omega+\mu|^3\right]. \tag{43}$$

We again use Eqs. (18) and (24) to obtain the impurity conductivity, denoted as $\sigma^c_{\mathrm{SP}}(T)$. The resistivity $\rho^c_{\mathrm{SP}}(T) = 1/\sigma^c_{\mathrm{SP}}(T)$. For temperature dependence we use the approximation $-\int g(\epsilon)\partial f/\partial\epsilon \simeq \int_{\mu-T}^{\mu+T} g(\epsilon)/2T$ in Eq. (24) to extract the leading order. To perform this computation we need to find the ω dependence in the principal integral of Eq. (43). This is done by fitting numerically the principal value of the integral for large $\Lambda/(\omega+\mu)$. This is because the relevant integration region for ω in the expression of conductivity is $\omega \subset (-T,T)$, which makes $\Lambda \gg |\omega+\mu|$ in our discussion. From the numerical fit with $10 < \frac{\Lambda^2}{(\omega+\mu)^2} < 10^2$ (chosen for an experimentally accessible range) we have

$$P\int_0^{\frac{\Lambda^2}{(\omega+\mu)^2}}\frac{x\,dx}{x-1} \simeq 2.589 + 1.022\frac{\Lambda^2}{(\omega+\mu)^2}.$$

The conductivity obtained is

$$\sigma^c_{\mathrm{SP}}(T) \simeq \frac{2e^2}{3}\frac{4v_F^2}{9\pi a_0^2 t^2}\int_{\mu-T}^{\mu+T} d\epsilon|\epsilon|\frac{\tau^c_{\mathrm{SP}}(\epsilon-\mu)}{2T},$$

$$\frac{1}{\tau^c_{\mathrm{SP}}(\epsilon-\mu)} = -\frac{2n_I}{\hbar}\frac{V^2|\epsilon|^2}{2t^2}\sum_s \mathrm{Im}\big[G^R_{dd,s}(\epsilon-\mu)\big].$$

For $0 < \mu \leqslant T$, the resistivity $\rho^c_{\mathrm{SP}}(T) = 1/\sigma^c_{\mathrm{SP}}(T) \to 0$ similar to the case for spin fluctuation in Eq. (36). For $T < \mu$ we have

$$\rho^c_{\mathrm{SP}}(T) = \frac{27\pi\alpha}{8}\frac{h}{e^2}n_I\frac{3\pi T\alpha(T^2-\mu^2)^5}{t^2 r^c_{\mathrm{SP}}(\mu,T)}$$

$$r^c_{\mathrm{SP}}(\mu,T) = T((a^4+\pi^2)\alpha^2T^{12}/t^4+\cdots) + 3a^2\frac{\alpha}{t^2}(\tilde{\epsilon}_d+\mu)(\mu^2-T^2)^5\ln\left(\frac{\mu-T}{\mu+T}\right). \tag{44}$$

Here $a = 2.589$ is the parameter from principal integral of the dot self-energy. We find the nonmagnetic region from Eq. (41) and study the temperature variation of resistivity within this charge fluctuation regime ($0 \leqslant n_s \ll 0.5$).

C. Range of validity for mean-field result

Before we proceed to compare the temperature dependences of resistivity due to charge fluctuations, spin fluctuations, and the influence of the impurity position, we pause here to discuss the regimes where mean-field results are valid in this Anderson impurity model. The order parameter of this unrestricted Hartree-Fock is the d-level occupation for a given spin $n_{d,s}$. To make a comparison with exact d-level occupation done by a Bethe ansatz,[26] we need to go back to the case for the conventional metal where the mean-field results were done by Anderson.[23] The d-level occupation for a given spin s at zero temperature is

$$n_{d,s} = \frac{1}{\pi}\cot^{-1}\left(\frac{\epsilon_d + Un_{d,-s} - \epsilon_F}{\Delta}\right). \tag{45}$$

Here $\Delta = \pi V^2\rho(\epsilon_F)$, with $\rho(\epsilon_F) = 1/2\pi$ the DOS for conventional metal. We solve Eq. (45) in the nonmagnetic region, where $n_{d,s} = n_{d,-s}$, and compare the answers with the exact results obtained by the Bethe ansatz. The comparison for d-level occupation for a given spin versus impurity level, with $\epsilon_F = 0$, is shown in Fig. 5.

From this figure we can see that the mean-field results deviate from the exact ones in a range $n_{d,s} \sim 0.06$–0.1 for the range of $U \sim 2$–8Δ, indicating that the mean field is a good approximation when the impurity level ϵ_d is higher than the Fermi energy ϵ_F or, in the other words, the impurity is near

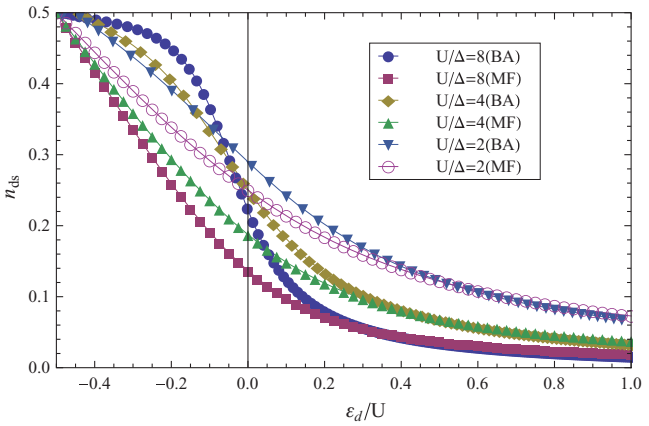

FIG. 5. (Color online) Comparison of Bethe ansatz with mean-field d-level occupation vs impurity level for conventional metal. The Fermi energy is set at $\epsilon_d = 0$. Lines denoted BA mean the Bethe ansatz results and lines denoted MF mean the mean-field results. The two match better in the region where $n_{ds} \leqslant 0.1$. This upper bound increases with decreasing U/Δ.

the empty orbital region. For larger Coulomb repulsion U/Δ the minimum value of ϵ_d of the overlapping region is closer to ϵ_F. Since for a two-dimensional system the mean-field results are marginal, we expect the mean-field result works for $\epsilon_d \simeq \epsilon_F = \mu$, as the s-wave scattering in the conventional metal considered above[23,26] is a one-dimensional problem. Since the crossover shifts to increasingly lower values of n_d as U increases, this is a rough criterion but establishes a basis for the mean-field calculations.

V. RESISTIVITY TEMPERATURE DEPENDENCE

In Secs. III and IV we have shown the analytic results of the temperature dependence of resistivity for $\beta\mu \gg 1$ and $\beta\mu \ll 1$. Here we compute numerically the temperature dependence of resistivity due to spin fluctuations, $\rho^s_{\rm SB}(T)$ and $\rho^s_{\rm SP}(T)$, for impurities breaking and preserving the honeycomb lattice symmetry, and the temperature dependence of resistivity due to charge fluctuations, $\rho^c_{\rm SB}(T)$ and $\rho^c_{\rm SP}(T)$. We use the full form of $R_{\rm SB}(\omega)$ and $R_{\rm SP}(\omega)$ and extract the results for $T > T_k$, with T_k obtained numerically the same way as we obtain the Kondo temperature in Figs. 2 and 4. We compare the resistivity for different symmetries with the same sets of parameters. The resistivity due to symmetry preserving impurities is much smaller than that of the symmetry breaking case due to the factor of $(\mu/t)^2$ [see Eqs. (20) and (33)]. We examine the resistivity due to impurity spin and charge fluctuations in the symmetry breaking case and make a comparison with the experimental results[1] in the next section.

A. Comparison of resistivity due to spin and charge fluctuations with different symmetry

We use $t = 2.7$ eV, $\Lambda = 3.5$ eV, $V = 1$ eV, and $U = 4$ eV in all of the numerical results within this section. We choose a different impurity level ϵ_d to explore the resistivity due to spin and charge fluctuations. The resistivity versus temperature is evaluated numerically between $T \subset (10^{-4}, 10^{-1})$ eV.

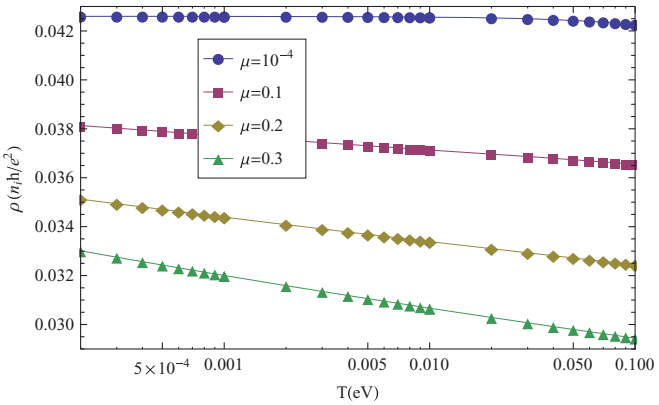

FIG. 6. (Color online) Perturbation results for resistivity vs temperature for the symmetry breaking case with $\epsilon_d = -1$ and various μ. The exchange coupling strength $|J|$ is larger than 0.2432 (for $\mu = 0.3$ eV) and less than 0.2884 eV (for $\mu = 10^{-4}$ eV) in the range chosen. In all cases the Kondo temperature is less than 10^{-12} eV, so the temperature range chosen is well above the Kondo scale.

Let us first study the local moment region. We choose $\epsilon_d = -1$ eV to ensure the d-level occupation $n_{d,s} \simeq 0.5$. The chemical potential μ is chosen between 10^{-4} and 0.3 eV. From $|J| \simeq \frac{V^2|U|}{|(\epsilon_d-\mu)(\epsilon_d+U-\mu)|}$ this choice of parameters renders the exchange coupling strength 1.14 eV $< |J| <$ 1.33 eV. For both cases these exchange coupling strengths are less than the critical value $|J_c|$, and the Kondo temperature T_k obtained for both cases is extremely small ($T_k < 10^{-12}$ eV). With this choice of parameters, $T_k \ll \mu$, and therefore the analytic expression for T_k corresponds to Eq. (23) for the symmetry breaking case and Eq. (35) for the symmetry preserving case. The resistivity versus temperature are plotted in Figs. 6 and 7.

In Fig. 6 we see the $T_k \ll T$ tails of the logarithmic upturns occurring when $T \simeq T_k$. The resistivity goes down as the chemical potential increases. This tendency is quite different from the case of the symmetry preserving ones, shown in Fig. 7.

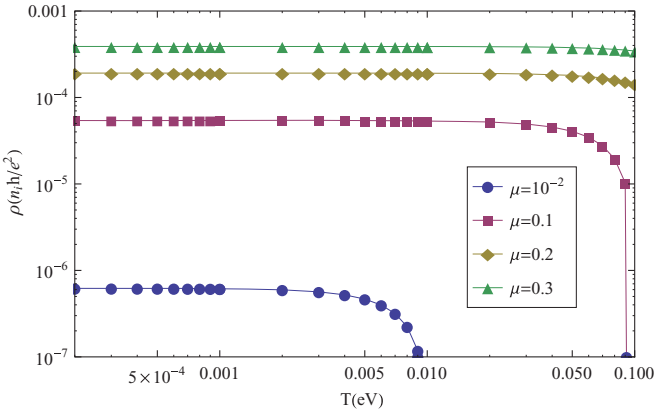

FIG. 7. (Color online) Perturbation results for resistivity vs temperature for the symmetry preserving case with $\epsilon_d = -1$ and various μ. The exchange coupling strength $|J|$ is larger than 0.2889 (for $\mu = 0.3$ eV) and less than 0.3380 eV (for $\mu = 10^{-2}$ eV) in the range chosen. In all cases the Kondo temperature is less than 10^{-12} eV, so the temperature range chosen is well above the Kondo scale.

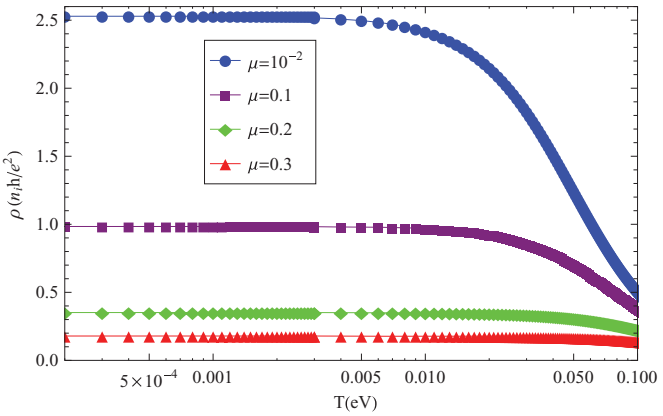

FIG. 8. (Color online) Mean-field results for resistivity vs temperature for the symmetry breaking case with $\epsilon_d = 0$ and various μ. The d-level occupation $n_{d,s}$ is greater than 0.024 (when $\mu = 10^{-2}$ eV) and less than 0.093 (when $\mu = 0.3$ eV) in the chosen range.

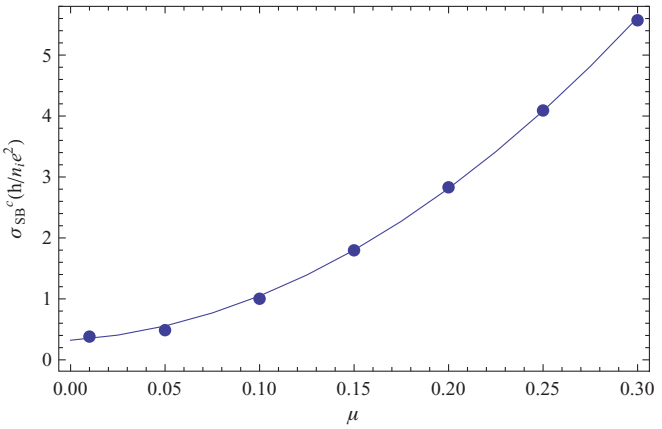

FIG. 9. (Color online) Mean-field results for conductivity at $T = 10^{-4}$ eV vs chemical potential μ (in units of eV). The symbols are the numerical data of conductivity at various chemical potentials and the line is the fitted quadratic curve with $\sigma \simeq 0.32 + 2.08\mu + 51.86\mu^2$. This quadratic behavior is also seen in Fig. 3(d) of Ref. 1.

The dependence of resistivity on chemical potential μ for the symmetry preserving case shows $\rho^s_{\rm SP}(\mu) \propto \mu^2$ by comparing the resistivity at $T = 10^{-4}$ eV in Fig. 7. At temperatures higher than the chemical potential, the resistivity decreases with increasing temperature faster than the logarithmic tail for all cases in Fig. 7. This is due to the divergence in conductivity when $\mu \simeq T$. The order of magnitude of resistivity at the same temperature for the symmetry preserving case is much smaller than the resistivity for the symmetry breaking case. Thus we can safely ignore the contributions from the symmetry preserving type of impurities when considering the resistivity due to spin fluctuations.

For the case of charge fluctuations we choose $\epsilon_d = 0$ eV to ensure the d-level occupation $n_{d,s} < 0.1$. The chemical potential μ is chosen between 10^{-4} and 0.3 eV. We compute the resistivity v.s. temperature for $T \subset (10^{-4}, 10^{-1})$ eV numerically from the mean-field results. The resistivity versus temperature are plotted in Figs. 8 and 10 for the symmetry breaking and symmetry preserving cases.

Figure 8 shows $\rho^c_{\rm SB}(T) \propto \ln(T)$ for $T > 10^{-2}$ eV and tends to a flat region for small temperature, which is very similar to the screening result of the Kondo effect at $T < T_k$. Conductivity at $T = 10^{-4}$ shows a quadratic chemical potential dependence, shown in Fig. 9, consistent with the gate voltage dependence on conductivity seen in the experiment.[1] The experimental fit in Ref. 1 for the Kondo scale, however, is approximately one order of magnitude smaller as compared with the energy scale obtained in the logarithmic temperature range in Fig. 8. The temperature dependence of resistivity in this charge fluctuation regime is similar to that of the Kondo model in this case, but the physics is not related to spin but charge fluctuation. To facilitate comparing our results with experimental ones in Ref. 1, we refer to the energy scale as a Kondo-like temperature in the following discussion.

Figure 10 also shows $\rho^c_{\rm SP}(T) \propto \ln(T)$ for $T \leqslant \mu$ with a shorter range of temperature and similarly tends to a flat region for small temperature. The resistivity increases with increasing chemical potential in Fig. 10, similar to the case of spin fluctuation. The resistivity for the symmetry preserving case is much smaller than that for the symmetry breaking impurities and thus ignores the contribution from symmetry preserving impurities.

In summary, when both types of impurities are present, the resistivity due to impurities preserving lattice symmetry is much smaller than that from impurities breaking the symmetry. Thus we focus our discussions on symmetry breaking cases for spin and charge fluctuations in the next section.

VI. COMPARISON WITH EXPERIMENTAL DATA

Here we make comparisons with the experimental data given in Ref. 1. We start with the perturbative results of the Kondo model in the case of impurities breaking the honeycomb symmetry. To have a large Kondo temperature (30 K $\leqslant T_k \leqslant$ 90 K in the experiment) the exchange coupling $|J|$ must be very close to its critical value $|J_c|$. As the perturbation breaks down when $T \sim T_k$, we can only analyze the gate voltage dependence of the Kondo temperature shown in Fig. 4 of Ref. 1. The strategy is the following: We find the

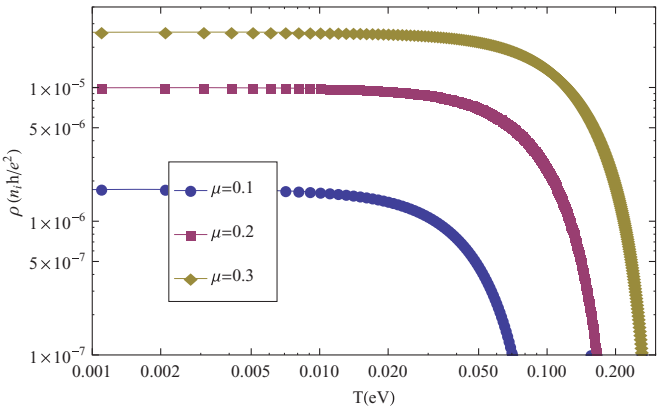

FIG. 10. (Color online) Mean-field results for resistivity vs temperature for the symmetry preserving case with $\epsilon_d = 0$ and various μ. The d-level occupation $n_{d,s}$ is greater than 0.040 (when $\mu = 0.1$ eV) and less than 0.093 (when $\mu = 0.3$ eV) in the chosen range.

TABLE I. Relationship between μ and ϵ_d obtained by fitting with the experimental Kondo temperature. The left two columns show the experimental Kondo temperature at a given gate voltage. We compute the corresponding chemical potential in the third column by using $V_g = 5.3 + 515.387\mu^2$. The impurity level ϵ_d, shown in the last column, is obtained by evaluating the corresponding exchange coupling strength J.

T_k (K)	V_g (V)	μ (eV)	ϵ_d (eV)
31.5	5.3	0	−0.225 949
32	6	0.0368 538	−0.191 582
35	10	0.095 495 3	−0.140 059
40	12.5	0.118 195	−0.119 956
51	15	0.137 189	−0.102 273
56.2	20	0.168 885	−0.074 372 7

impurity level ϵ_d at a given chemical potential μ by using the experimental Kondo temperature T_k as the Kondo temperature obtained by the pole of resistivity, or $1 + J R_{\rm SB}(0) = 0$, where $J \simeq V^2/(\epsilon_d - \mu)(\epsilon_d + U - \mu)$.

In the experiment the Kondo temperature is obtained as a function of gate voltage. We assume the gate voltage V_g is connected with chemical potential μ via a capacitive effect, i.e., $Q/e = c_g V_g/e = 8c_g\mu^2/(27\sqrt{3}\pi t^2 a_0^2)$, with Q representing the electric charges, $e = 1.6 \times 10^{-19}$ C, and $c_g = 1.15 \times 10^{-8}$ F/cm^2 as the capacitance of the graphene. In the experiment of Ref. 1, $V_g = 5.3$ V is regarded as the position of the Dirac node. Thus we take $V_g = 5.3 + 8e/(27\sqrt{3}\pi t^2 a_0^2 c_g)\mu^2 = 5.3 + 515.387\mu^2$ by fixing $V_g = 5.3V$ at $\mu = 0$ eV. Using the experimental Kondo temperature at a given chemical potential, we compute the corresponding exchange coupling strength J and thus determine the relationship between μ and impurity level ϵ_d. The results are shown in Table I.

From Table I we find $\epsilon_d \propto \mu$. The obtained impurity level ϵ_d changes linearly with the chemical potential μ, as shown in lower left-hand side of Fig. 11. One of the main conclusions of this work is that the observed upturn in resistivity[1] can be understood in terms of an Anderson impurity model only if the impurity level varies with the applied voltage. By using the linear fit in this figure, we obtain the Kondo temperature as a function of chemical potential as shown in the top of Fig. 11. Between $\mu = 0.02$ and 0.3 eV the Kondo temperature grows monotonically from 14 to 90 K. The decrease of T_k with increasing μ for 0 eV $< \mu <$ 0.02 eV may indicate the failure of linearity between μ and ϵ_d for the onset of nonzero chemical potential or the failure of the Kondo physics near the node. The chemical potential dependence shown in top figure of Fig. 11 is roughly consistent with Fig. 4 in Ref. 1 in the intermediate gate voltage.

For gate voltage V_g larger than 30 V in Ref. 1, the experimental T_k begins to decrease with increasing gate voltage. This can be accounted for qualitatively, as shown in Fig. 12, by assuming that the energy of the impurity level no longer changes with the external gate voltage for $V_g > 30$ V due to sufficient charge screening. For a small gate voltage (chemical potential close to the node) the experimental T_k increases monotonically with increasing gate voltage. In this region neither a constant impurity level nor $\epsilon_d \propto \mu$ gives the

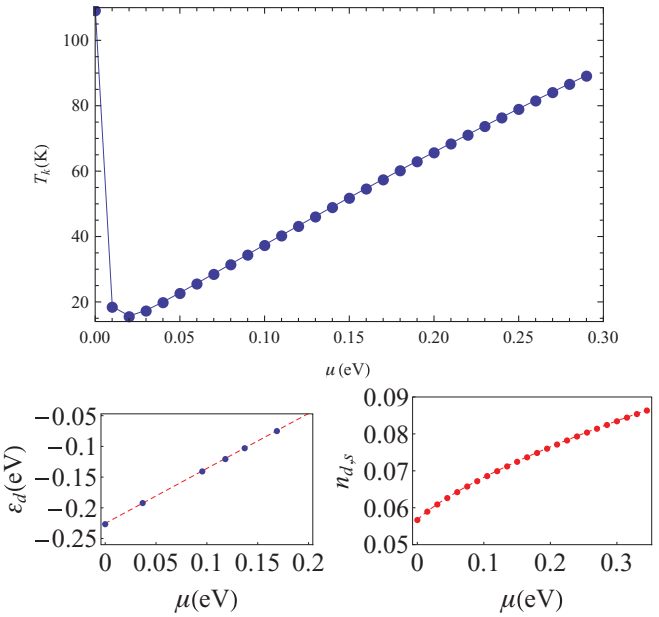

FIG. 11. (Color online) Top: Kondo temperature T_k as a function of chemical potential μ. The relationship is obtained by $|J| \sim V^2/|\mu - \epsilon_d|$ and $\epsilon_d \propto \mu$, which we find by fitting the experimental data shown in the lower left-hand figure. Lower left-hand side: Impurity level ϵ_d as a function of chemical potential. The symbols are obtained by the data in Fig. 4 of Ref. 1 shown in Table I. The red dashed line is the linear fitting function which gives $\epsilon_d = -0.2254 + 0.8951\mu$. Lower right-hand side: Impurity occupation of a given spin $n_{d,s}$ as a function of chemical potential evaluated by the mean-field approach.

corresponding experimental dependence on V_g based on our perturbative Kondo results.

We also compute the impurity occupation as a function of μ by using the mean field as shown by Eq. (41) in the symmetry breaking case. The obtained impurity occupation for a given spin increased from 0.057 to 0.082 monotonically between $\mu \subset$ (0,0.3) eV. Given that the validity of the mean field is limited to small values of the impurity level occupations (see

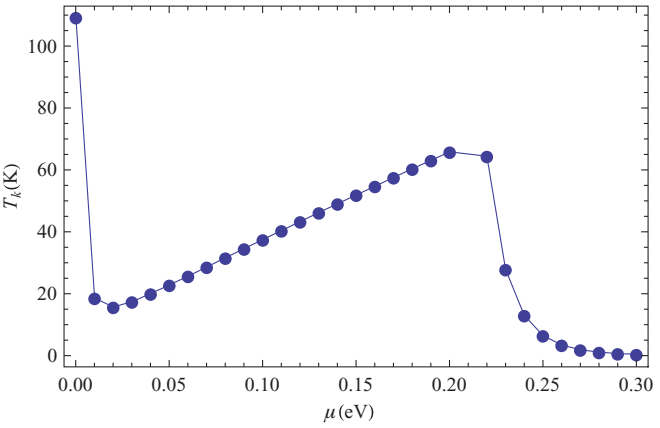

FIG. 12. (Color online) Kondo temperature T_k as a function of chemical potential μ. The relationship is obtained by $|J| \sim V^2/|\mu - \epsilon_d|$ and $\epsilon_d = -0.2254 + 0.8951\mu$ for $0 \leqslant \mu \leqslant 0.21$ eV and $\epsilon_d = -0.029\,456$ (corresponds to $V_g = 30^{\sim}V$ or $\mu = 0.2189$ eV) for 0.21 eV $< \mu \leqslant$ 0.3 eV.

Sec. IV C), we expect deviations away from the mean field. Thus the system is not likely to stay in the local moment region near the node, suggesting a crossover of impurity occupation from the local moment to the empty orbital regime based on the NRG results in Ref. 15. Thus the Kondo effect alone would not be able to explain the logarithmic temperature dependence seen in Ref. 1.

Let us now investigate whether charge fluctuations can give rise to a temperature dependence of resistivity seen in the experiment. We take $\epsilon_d = -0.2254 + 0.8951\mu$ and evaluate the resistivity versus temperature from the mean-field results of the impurity Green's function for the symmetry breaking case. For a chemical potential close to the node, we get a reasonable temperature scale (the logarithmic behavior shows up at $T \simeq 10^{-3}$ eV) from charge fluctuations as shown in the top figure of Fig. 13. We also have μ^2 being proportional to conductivity at zero temperature, as seen in the lower left-hand side of Fig. 13, which was observed in Ref. 1. Rescaling $\rho(T)$ by $\rho(0)$ and T by the Kondo-like temperature T_k^c obtained by the temperature at which the resistivity begins to show a logarithmic dependence in T, we obtain the universal curve shown in the lower right-hand side of Fig. 13. In this range of chemical potential the impurity occupation $n_{d,s} \simeq 0.057$. It shows that even for the chemical potential μ close to the node, the one-parameter scaling is still possible in this charge fluctuation scheme, while as it is shown analytically in Eq. (25), the one-parameter scaling is unlikely for $\mu \simeq 0$ in the Kondo case.

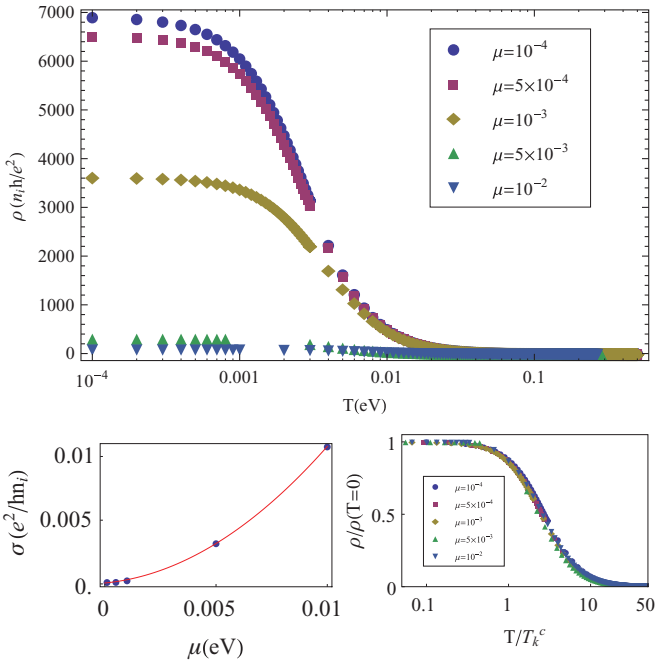

FIG. 13. (Color online) Top: Resistivity vs temperature for the charge fluctuation case with $\epsilon_d = -0.2254 + 0.8951\mu$ and a chemical potential between 10^{-4} and 10^{-2} eV. Lower left-hand side: Quadratic dependence on μ for conductivity at zero temperature. The red line is the quadratic fitting which gives $\sigma_{\rm SB}^c(\mu, T=0) = 0.000\,0693 + 0.1675\mu + 90.3726\mu^2$ and the blue symbols are conductivity at various chemical potentials. Lower right-hand side: Universality curve after rescaling resistivity and Kondo-like temperature scale T_k^c obtained by the temperature scale when logarithmic behavior is shown. $1.1T_k^c \simeq T_k$ by comparing this universality curve with Fig. 2(b) in Ref. 1.

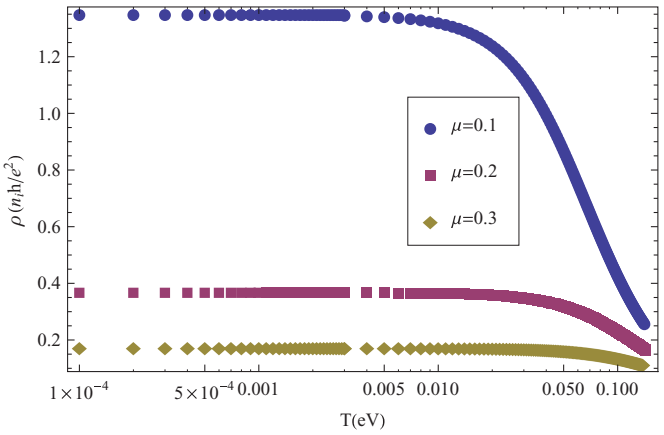

FIG. 14. (Color online) Resistivity due to charge fluctuations vs temperature plot. For $T < 10^{-2}$ eV the resistivity decreases slowly with temperature. For 10^{-2} eV $< T$ the logarithmic dependence on temperature begins to appear.

For chemical potentials away from the Dirac node we plot the resistivity versus temperature for $\mu = 0.1$, 0.2, and 0.3 eV in Fig. 14. The overall feature is very similar to the Kondo results: Near zero temperature the resistivity decreases with T^2 while at large temperature $\rho(T) \propto \ln(T)$. At zero temperature the conductivity is proportional to μ^2 as in the case shown in Fig. 9. However, the logarithmic behavior shows up at $T \simeq 10^{-2}$ eV, which is approximately one order of magnitude larger than the experimental results in Ref. 1. Thus the charge fluctuation cannot explain the experiment for large chemical potentials.

By comparing the universal curve obtained by NRG[24] shown in Fig. 2(b) in Ref. 1 and the one we have for charge fluctuations in lower right-hand side of Fig. 13, we get $1.1T_k^c \sim T_k$. The "Kondo temperature" for both charge and spin fluctuations as a function of chemical potential is shown in Fig. 15. From Fig. 15 we observe that charge fluctuations give a large Kondo scale with increasing chemical potential and good agreement with experimental results is obtained only if $\mu \leqslant 10^{-3}$ eV. Away from the node, the Kondo scale obtained by charge fluctuations grows much faster than that of the spin fluctuations. The Kondo scale obtained from spin fluctuation, on the other hand, gives a large Kondo scale for $\mu < 10^{-2}$ eV and reaches its minimum when $\mu \sim 0.02$ eV. The combined picture of the two cases as shown in Fig. 15, by assuming charge fluctuation for $\mu \sim 0$ and spin fluctuation for large μ, can give an overall consistent picture as seen in the experiment for gate voltages of less than 30 V. For 10^{-3} eV $< \mu < 0.06$ eV it shows the crossover from charge fluctuations to spin fluctuations, which is not accounted for in our simple mean field in Anderson model nor perturbation in the Kondo model. For gate voltages of larger than 30 V a nonmonotonic dependence of T_k on μ is seen in Ref. 1. Given our analysis, we speculate that the screening due to the finite density of carriers could modify the dependence of the energy of the impurity level on the gate voltage. A weaker

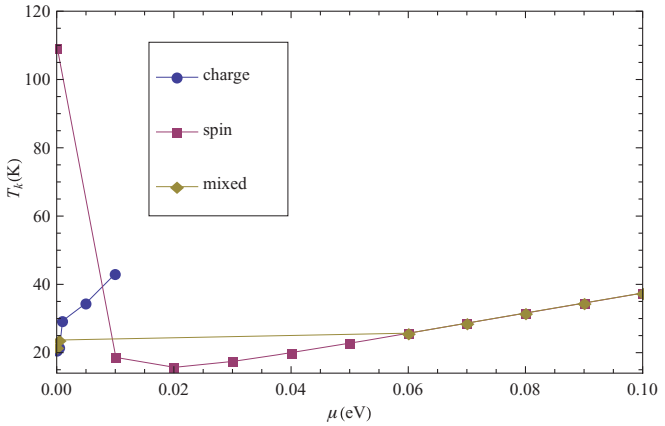

FIG. 15. (Color online) Kondo temperature T_k as a function of chemical potential μ. The blue symbols are the Kondo-like temperature, obtained by comparing the universal curve with NRG results, for the charge fluctuation case. The purple symbols are the Kondo temperature for the spin fluctuation case. Between $\mu = 10^{-3}$ and 0.02 eV, both cases give a Kondo temperature higher than their neighboring chemical potentials. The "mixed" (brown symbols) case takes the Kondo scale obtained by charge fluctuations with $\mu < 10^{-3}$ eV and spin fluctuations with $\mu > 0.02$ eV. By combing these two, the Kondo scale obtained grows monotonically with chemical potential.

dependence at a large gate voltage will lead to a decreasing Kondo temperature.

VII. CONCLUSION

We use the Anderson impurity model to describe the dilute impurity behavior in graphene. The goal is to test whether the recent experiment on the resistivity of graphene with vacancies induced by ion irradiation in ultrahigh vacuum[1] can be solely explained by the single impurity Kondo effect (spin fluctuations). To study this local moment regime we use the Schrieffer-Wolf transformation to freeze the charge degrees of freedom and obtain the Kondo Hamiltonian. In the case of dilute impurities we may ignore the RKKY interactions and treat the problem as a single impurity Kondo model.

We have computed this Kondo contribution to dc resistivity by perturbation in a T-matrix formulation. Analytic expressions are obtained for $\beta\mu \ll 2\pi$ and $\beta\mu \gg 2\pi$ by taking the asymptotic form of the digamma function in the integrand. The Kondo temperature dependence on chemical potential and exchange coupling is obtained. Depending on the location of the impurities, the Kondo contribution to resistivity is very different. For the type of magnetic impurities which break the C_{3v} symmetry at low chemical potentials, it shows a power-law temperature dependence as $1/(T - T_k)$. For the magnetic impurities preserving the C_{3v} symmetry of the lattice at low chemical potentials, it shows a power-law dependence as $1/(T^3 - T_k^3)$. At even lower chemical potentials when the Fermi surface is close to the node, both cases show an extra dependence on the chemical potential as well as the Kondo scale. Near the node a critical value of exchange coupling is needed for the Kondo effect to be realized.[13,15] The critical value $|J_c|$ is larger for the symmetry breaking case. For a large chemical potential μ both cases show logarithmic dependence on temperature scaled by the Kondo temperature. With increasing μ the resistivity at a given temperature decreases for impurities breaking the honeycomb symmetry while the resistivity increases for the ones preserving the symmetry. The resistivity obtained with the same set of parameters shows that the dominant source of resistivity is from the impurities which break the C_{3v} symmetry.

We have also computed the effect of charge fluctuation for impurity occupation $0 \leqslant n_{d,s} \ll 0.5$ by using the mean-field approach on the Anderson impurity model. The resistivity at a given temperature has a similar dependence on the chemical potential as the case for spin fluctuations. Similar to the spin fluctuation case, the dominant contribution to resistivity at the same sets of parameters comes from the impurities which break the honeycomb lattice symmetry.

By studying the resistivity versus temperature and comparing with the experimental results in Ref. 1 from both spin and charge fluctuations in the symmetry breaking case, we find that the Kondo effect fails to give the correct Kondo scale and is unable to describe single-parameter scaling for a chemical potential near the node. For $\mu \sim 0$ the resistivity due to charge fluctuations gives a reasonable temperature dependence and the resistivity after rescaling also shows a single-parameter universal behavior. The same analysis yields a large Kondo scale for 10^{-2} eV $< \mu$ in the charge fluctuation case, which is roughly the same chemical potential at which we obtain nonmonotonic behavior of the Kondo temperature in the spin fluctuation (Kondo) case.

The failure of a Kondo explanation near the node is consistent with the NRG results,[14] which find that the Kondo effect near the node is suppressed for $r > 1/2$ for systems having an electronic density of state $\rho(\epsilon) \propto |\epsilon|^r$. By combining the low chemical potential results ($0 \leqslant \mu \leqslant 10^{-3}$ eV) from charge fluctuation with the large 10^{-2} eV $< \mu$ results from the Kondo effect, we obtain a Kondo scale consistent with the experimental results. For a chemical potential in between these two cases, the system should be in the mixed valence regime. For gate voltages of higher than 30 V, a weaker dependence of the impurity energy on the applied gate voltage as compared to the dependence at smaller chemical potentials will lead to a decrease in the Kondo temperature. Whether this effect or the effect of RKKY interactions is responsible for the observed nonmonotonic behavior on gate voltage will be the subject of future studies.

ACKNOWLEDGMENTS

The authors wish to acknowledge Roland Kawakami and Shan-Wen Tsai for useful discussions. The authors' research is supported by the University of California at Riverside under an initial complement.

APPENDIX A: DERIVATION FOR SYMMETRY BREAKING CASE

$$R_{\rm SB}(z) = \frac{4}{9\pi t^2}\int_{-\infty}^{\infty}\frac{|\epsilon|d\epsilon}{\epsilon-(z+\mu)}\tanh\left(\frac{\epsilon-\mu}{2k_BT}\right)\frac{\Lambda^2}{\epsilon^2+\Lambda^2}.$$

Defining $y = \epsilon - \mu$ and using

$$\tanh\left(\frac{\beta y}{2}\right) = \frac{1}{i\pi}\left[\psi\left(\frac{1}{2} + i\frac{\beta y}{2\pi}\right) - \psi\left(\frac{1}{2} - i\frac{\beta y}{2\pi}\right)\right].$$

As $\psi(\frac{1}{2} \pm i\frac{\beta y}{2\pi})$ has poles on upper and/or lower complex plane, we may separate $R_{\rm SB}(z)$ into two parts as $R_{\rm SB}(z) = (I_1 + I_2)4/(9\pi t^2)$, with I_1 and I_2 given by

$$I_1 = \frac{1}{i\pi}\int_{-\infty}^{\infty} dy \frac{|y+\mu|}{y-z}\frac{\Lambda^2}{(y+\mu)^2+\Lambda^2}\psi\left(\frac{1}{2} + i\frac{\beta y}{2\pi}\right), \quad I_2 = \frac{-1}{i\pi}\int_{-\infty}^{\infty} dy \frac{|y+\mu|}{y-z}\frac{\Lambda^2}{(y+\mu)^2+\Lambda^2}\psi\left(\frac{1}{2} - i\frac{\beta y}{2\pi}\right).$$

We may write $I_1 = I_{11} + I_{12}$ with

$$\begin{aligned} I_{11} &= \frac{-1}{i\pi}\int_{-\infty}^{\mu} dy \frac{y+\mu}{y-z}\frac{\Lambda^2}{(y+\mu)^2+\Lambda^2}\psi\left(\frac{1}{2} + i\frac{\beta y}{2\pi}\right) = -\frac{\Lambda}{2\pi}\int_{-\infty}^{-\mu} dy \frac{y+\mu}{y-z}\left(\frac{\psi\left(\frac{1}{2}+i\frac{\beta y}{2\pi}\right)}{y+\mu+i\Lambda} - \frac{\psi\left(\frac{1}{2}+i\frac{\beta y}{2\pi}\right)}{y+\mu-i\Lambda}\right) \\ &= \left\{\frac{\Lambda}{2\pi} i\pi \frac{-i\Lambda}{-i\Lambda-(z+\mu)}\psi\left(\frac{1}{2} - i\frac{\beta\mu}{2\pi} + \frac{\beta\Lambda}{2\pi}\right) + \frac{\Lambda}{2\pi}\int_0^{-\Lambda+\delta} i\,dx \frac{ix}{ix-(z+\mu)}\frac{1}{i(x+\Lambda)}\psi\left(\frac{1}{2} - i\frac{\beta\mu}{2\pi} - \frac{\beta x}{2\pi}\right)\right. \\ &\quad \left. + \frac{\Lambda}{2\pi}\int_{-\Lambda-\delta}^{-\infty} i\,dx \frac{ix}{ix-(z+\mu)}\frac{1}{i(x+\Lambda)}\psi\left(\frac{1}{2} - i\frac{\beta\mu}{2\pi} - \frac{\beta x}{2\pi}\right)\right\} + \frac{\Lambda}{2\pi}\int_{-\infty}^{-\mu} dy \frac{y+\mu}{y-z}\frac{\psi\left(\frac{1}{2}+i\frac{\beta y}{2}\right)}{y+\mu-i\Lambda}. \end{aligned}$$

In the third and fourth lines of the above equation we replaced y by $y = -\mu + ix$ and $\delta \to +0$. A similar computation gives I_{12} as

$$\begin{aligned} I_{12} &= \frac{\Lambda}{2\pi}\int_{-\mu}^{\infty} dy \frac{y+\mu}{y-z}\left(\frac{\psi\left(\frac{1}{2}+i\frac{\beta y}{2\pi}\right)}{y+\mu+i\Lambda} - \frac{\psi\left(\frac{1}{2}+i\frac{\beta y}{2\pi}\right)}{y+\mu-i\Lambda}\right) \\ &= \left(-\frac{\Lambda}{2\pi}\right)\left\{\int_{-\infty}^{-\Lambda-\delta} i\,dx \frac{ix}{ix-(z+\mu)}\frac{\psi\left(\frac{1}{2}-i\frac{\beta\mu}{2\pi}-\frac{\beta x}{2\pi}\right)}{i(x+\Lambda)} + \int_{-\Lambda+\delta}^{0} i\,dx \frac{ix}{ix-(z+\mu)}\frac{\psi\left(\frac{1}{2}-i\frac{\beta\mu}{2\pi}-\frac{\beta x}{2\pi}\right)}{i(x+\Lambda)}\right\} \\ &\quad - i\pi\frac{\Lambda}{2\pi}\frac{i\Lambda}{(\mu+z)+i\Lambda}\psi\left(\frac{1}{2} - i\frac{\beta\mu}{2\pi} + \frac{\beta\Lambda}{2\pi}\right) - \frac{\Lambda}{2\pi}\int_{-\mu}^{\infty} dy \frac{y+\mu}{y-z}\frac{\psi\left(\frac{1}{2}+i\frac{\beta y}{2\pi}\right)}{y+\mu-i\Lambda}. \end{aligned}$$

Combining I_{11} and I_{12} we get

$$I_1 = \frac{\Lambda}{2\pi}\int_{\bar{C}_1} d\bar{z}\frac{\bar{z}+\mu}{\bar{z}-z}\left(\frac{\psi\left(\frac{1}{2}+i\frac{\beta\bar{z}}{2\pi}\right)}{\bar{z}+\mu-i\Lambda}\right)2 - \frac{\Lambda}{i\pi}\left(\int_{-\infty}^{-\Lambda-\delta} + \int_{-\Lambda+\delta}^{0}\right)dx\frac{x\psi\left(\frac{1}{2}-i\frac{\beta\mu}{2\pi}-\frac{\beta x}{2\pi}\right)}{(x+\Lambda)(z+\mu-ix)}.$$

Here $\bar{C}_1$ denotes the integration path taken from $\bar{z} = -\mu - i\infty$ to $\bar{z} = -\mu$ along the imaginary axis. We may also write $I_2 = I_{21} + I_{22}$ in a different region as

$$\begin{aligned} I_{21} &= \frac{1}{i\pi}\int_{-\infty}^{-\mu} dy \frac{y+\mu}{y-z}\frac{\Lambda^2}{(y+\mu)^2+\Lambda^2}\psi\left(\frac{1}{2} - i\frac{\beta y}{2\pi}\right) = \frac{\Lambda}{2\pi}\int_{-\infty}^{-\mu} dy \frac{y+\mu}{y-z}\left(\frac{\psi\left(\frac{1}{2}-i\frac{\beta y}{2\pi}\right)}{y+\mu+i\Lambda} - \frac{\psi\left(\frac{1}{2}-i\frac{\beta y}{2\pi}\right)}{y+\mu-i\Lambda}\right) \\ &= \frac{-\Lambda}{2\pi}\int_{\bar{C}_2} d\bar{z}\frac{\bar{z}+\mu}{\bar{z}-z}\frac{\psi\left(\frac{1}{2}-i\frac{\beta\bar{z}}{2\pi}\right)}{\bar{z}+\mu+i\Lambda} + \frac{\Lambda}{2\pi}\left(\int_0^{\Lambda-\delta} + \int_{\Lambda+\delta}^{\infty}\right)dx\frac{x\psi\left(\frac{1}{2}+i\frac{\beta\mu}{2\pi}+\frac{\beta x}{2\pi}\right)}{x+i(\mu+z)(x-\Lambda)} \\ &\quad -i\pi\frac{\Lambda}{2\pi}\frac{i\Lambda}{i\Lambda-(\mu+z)}\psi\left(\frac{1}{2} + i\frac{\beta\mu}{2\pi} + \frac{\beta\Lambda}{2\pi}\right). \end{aligned}$$

Here $\bar{C}_2$ denotes the integration path taken from $\bar{z} = -\mu$ to $\bar{z} = -\mu + i\infty$ along the imaginary axis. I_{22} is expressed as

$$\begin{aligned} I_{22} &= \frac{-1}{i\pi}\int_{-\mu}^{\infty} dy \frac{y+\mu}{y-z}\frac{\Lambda^2}{(y+\mu)^2+\Lambda^2}\psi\left(\frac{1}{2} - i\frac{\beta y}{2\pi}\right) = \frac{\Lambda}{2\pi}\int_{-\mu}^{\infty} dy \frac{y+\mu}{y-z}\left(\frac{\psi\left(\frac{1}{2}-i\frac{\beta y}{2\pi}\right)}{y+\mu-i\Lambda} - \frac{\psi\left(\frac{1}{2}-i\frac{\beta y}{2\pi}\right)}{y+\mu+i\Lambda}\right) \\ &= -\frac{\Lambda}{2\pi}2\pi i\frac{z+\mu}{z+\mu+i\Lambda}\psi\left(\frac{1}{2} - i\frac{\beta z}{2\pi}\right) - \frac{\Lambda}{2\pi}\int_{\bar{C}_2} d\bar{z}\frac{\bar{z}+\mu}{\bar{z}-z}\frac{\psi\left(\frac{1}{2}-i\frac{\beta\bar{z}}{2\pi}\right)}{\bar{z}+\mu+i\Lambda} - \frac{\Lambda}{2\pi}\left(\int_{\infty}^{\Lambda+\delta} + \int_{\Lambda-\delta}^{0}\right)dx\frac{x\psi\left(\frac{1}{2}+i\frac{\beta\mu}{2\pi}+\frac{\beta x}{2\pi}\right)}{[x+i(\mu+z)](x-\Lambda)} \\ &\quad + \frac{\Lambda}{2\pi}i\pi\frac{i\Lambda}{i\Lambda-(\mu+z)}\psi\left(\frac{1}{2} + i\frac{\beta\mu}{2\pi} + \frac{\beta\Lambda}{2\pi}\right) + \frac{\Lambda}{2\pi}2\pi i\frac{z+\mu}{z+\mu-i\Lambda}\psi\left(\frac{1}{2} - i\frac{\beta z}{2\pi}\right). \end{aligned}$$

The sum of I_1 and I_2 is then given by

$$R_{\rm SB}(z) = \frac{4}{9\pi t^2}(I_1+I_2) = \frac{4}{9\pi t^2}\Bigg[\frac{\Lambda}{\pi}\Bigg(\int_{\bar{C}_1} d\bar{z}\frac{\bar{z}+\mu}{\bar{z}-z}\frac{\psi\left(\frac{1}{2}+i\frac{\beta\bar{z}}{2\pi}\right)}{\bar{z}+\mu-i\Lambda} - \int_{\bar{C}_2} d\bar{z}\frac{\bar{z}+\mu}{\bar{z}-z}\frac{\psi\left(\frac{1}{2}-i\frac{\beta\bar{z}}{2\pi}\right)}{\bar{z}+\mu+i\Lambda}\Bigg)$$

$$-\frac{\Lambda}{\pi i}\left(\int_{-\infty}^{-\Lambda-\delta}+\int_{-\Lambda+\delta}^{0}\right)dx\frac{x\psi\left(\frac{1}{2}-i\frac{\beta\mu}{2\pi}-\frac{\beta x}{2\pi}\right)}{(z+\mu-ix)(x+\Lambda)} + \frac{\Lambda}{\pi i}\left(\int_{0}^{\Lambda-\delta}+\int_{\Lambda+\delta}^{\infty}\right)dx\frac{x\psi\left(\frac{1}{2}+i\frac{\beta\mu}{2\pi}+\frac{\beta x}{2\pi}\right)}{(z+\mu-ix)(x-\Lambda)}$$

$$+i\Lambda\psi\left(\frac{1}{2}-i\frac{\beta z}{2\pi}\right)\left(\frac{z+\mu}{z+\mu-i\Lambda}-\frac{z+\mu}{z+\mu+i\Lambda}\right)\Bigg].$$

Rewriting $\bar{z} = -\mu + ix$ in the expression of $R_{\rm SB}(z)$ along the $\bar{C}_1$ and $\bar{C}_2$ paths we get

$$R_{\rm SB}(z) = \frac{4}{9\pi t^2}\Bigg\{\frac{-\Lambda}{i\pi}\Bigg(\int_0^\infty dx\frac{x\psi\left(\frac{1}{2}+i\frac{\beta\mu}{2\pi}+\frac{\beta x}{2\pi}\right)}{(\mu+z-ix)(x+\Lambda)} - \int_0^\infty dx\frac{x\psi\left(\frac{1}{2}-i\frac{\beta\mu}{2\pi}+\frac{\beta x}{2\pi}\right)}{(\mu+z+ix)(x+\Lambda)}\Bigg)$$

$$+\frac{\Lambda}{i\pi}\left(\int_0^{\Lambda-\delta}+\int_{\Lambda+\delta}^{\infty}\right)dx\left[\frac{x\psi\left(\frac{1}{2}+i\frac{\beta\mu}{2\pi}+\frac{\beta x}{2\pi}\right)}{(\mu+z-ix)(x+\Lambda)} - \frac{x\psi\left(\frac{1}{2}-i\frac{\beta\mu}{2\pi}+\frac{\beta x}{2\pi}\right)}{(\mu+z+ix)(x+\Lambda)}\right] + \psi\left(\frac{1}{2}-i\frac{\beta z}{2\pi}\right)\left[\frac{-2\Lambda^2(z+\mu)}{(z+\mu)^2+\Lambda^2}\right]\Bigg\}.$$

By defining $F(x,\mu,z)$ as

$$F(x,\mu,z) = \frac{\psi\left(\frac{1}{2}+i\frac{\beta\mu}{2\pi}+\frac{\beta x}{2\pi}\right)}{x+i(\mu+z)} + \frac{\psi\left(\frac{1}{2}-i\frac{\beta\mu}{2\pi}+\frac{\beta x}{2\pi}\right)}{x-i(\mu+z)},$$

we may simplify the above expression as

$$R_{\rm SB}(z) = \frac{4}{9\pi t^2}\left[\frac{\Lambda}{\pi}\left(\mathrm{P}\int_0^\infty dx\frac{F(x,\mu,z)x}{x-\Lambda} - \int_0^\infty dx\frac{F(x,\mu,z)x}{x+\Lambda}\right) - \psi\left(\frac{1}{2}-i\frac{\beta z}{2\pi}\right)\frac{2\Lambda^2(z+\mu)}{(z+\mu)^2+\Lambda^2}\right]. \tag{A1}$$

APPENDIX B: DERIVATION FOR SYMMETRY PRESERVING CASE

Considering integrals of the form

$$R_{\rm SP}(z) = \frac{4}{9\pi t^4}\int_{-\infty}^{\infty}\frac{|\epsilon|^3 d\epsilon}{\epsilon-(z+\mu)}\tanh\left(\frac{\epsilon-\mu}{2k_BT}\right)\frac{\Lambda^4}{\epsilon^4+\Lambda^4},$$

and letting $y = \epsilon - \mu$, we get

$$R_{\rm SP}(z) = \frac{4}{9\pi t^4}\left\{\frac{1}{i\pi}\int_{-\infty}^{\infty}dy\frac{|y+\mu|^3}{y-z}\frac{\Lambda^4}{(y+\mu)^4+\Lambda^4}\left[\psi\left(\frac{1}{2}+\frac{i\beta y}{2\pi}\right)-\psi\left(\frac{1}{2}-\frac{i\beta y}{2\pi}\right)\right]\right\} = \frac{4}{9\pi t^4}(\bar{I}_1+\bar{I}_2).$$

We take the integration regions into two parts by writing $\bar{I}_1 = \bar{I}_{11} + \bar{I}_{12}$ with

$$\bar{I}_{11} = \frac{-1}{i\pi}\int_{-\infty}^{-\mu}dy\frac{(y+\mu)^3}{y-z}\frac{\Lambda^4}{(y+\mu)^4+\Lambda^4}\psi\left(\frac{1}{2}+\frac{i\beta y}{2\pi}\right) = \frac{-1}{i\pi}\Bigg\{-2\pi i\frac{\left(\Lambda e^{-\frac{3}{4}\pi i}\right)^3}{\Lambda e^{-\frac{3}{4}\pi i}-(z+\mu)}$$

$$\times\frac{\Lambda^4\psi\left(\frac{1}{2}-i\frac{\beta\mu}{2\pi}+i\frac{\beta\Lambda e^{-\frac{3}{4}\pi i}}{2\pi}\right)}{\Lambda^3\left(e^{-\frac{3}{4}\pi i}-e^{\frac{1}{4}\pi i}\right)\left(e^{-\frac{3}{4}\pi i}-e^{\frac{-1}{4}\pi i}\right)\left(e^{-\frac{3}{4}\pi i}-e^{\frac{3}{4}\pi i}\right)} - \int_0^{-\infty}dx\frac{x^3}{ix-(z+\mu)}\left[\frac{\Lambda^4\psi\left(\frac{1}{2}-i\frac{\beta\mu}{2\pi}-\frac{\beta x}{2\pi}\right)}{x^4+\Lambda^4}\right]\Bigg\},$$

$$\bar{I}_{12} = \frac{1}{i\pi}\int_{-\mu}^{\infty}dy\frac{(y+\mu)^3}{y-z}\frac{\Lambda^4}{(y+\mu)^4+\Lambda^4}\psi\left(\frac{1}{2}+\frac{i\beta y}{2\pi}\right) = \frac{1}{i\pi}\Bigg\{-2\pi i\frac{\left(\Lambda e^{-\frac{1}{4}\pi i}\right)^3}{\Lambda e^{-\frac{1}{4}\pi i}-(z+\mu)}$$

$$\times\frac{\Lambda^4\psi\left(\frac{1}{2}-i\frac{\beta\mu}{2\pi}+i\frac{\beta\Lambda e^{-\frac{1}{4}\pi i}}{2\pi}\right)}{\Lambda^3\left(e^{-\frac{1}{4}\pi i}-e^{\frac{1}{4}\pi i}\right)\left(e^{-\frac{1}{4}\pi i}-e^{\frac{3}{4}\pi i}\right)\left(e^{-\frac{1}{4}\pi i}-e^{\frac{-3}{4}\pi i}\right)} - \int_{-\infty}^{0}dx\frac{x^3}{ix-(z+\mu)}\left[\frac{\Lambda^4\psi\left(\frac{1}{2}-i\frac{\beta\mu}{2\pi}-\frac{\beta x}{2\pi}\right)}{x^4+\Lambda^4}\right]\Bigg\}.$$

Thus

$$\bar{I}_1 = \bar{I}_{11} + \bar{I}_{12} = \frac{\Lambda^4 \psi\left(\frac{1}{2} - i\frac{\beta\mu}{2\pi} + \frac{i\beta\Lambda e^{-\frac{3}{4}\pi i}}{2\pi}\right)}{2\left(\Lambda e^{-\frac{3}{4}\pi i} - (z+\mu)\right)} - \frac{\Lambda^4 \psi\left(\frac{1}{2} - i\frac{\beta\mu}{2\pi} + \frac{i\beta\Lambda e^{-\frac{\pi i}{4}}}{2\pi}\right)}{2\left(\Lambda e^{-\frac{\pi i}{4}} - (z+\mu)\right)}$$

$$+\frac{2}{i\pi}\int_0^{-\infty} dx \frac{x^3}{ix - (z+\mu)} \frac{\Lambda^4 \psi\left(\frac{1}{2} - i\frac{\beta\mu}{2\pi} - \frac{\beta x}{2\pi}\right)}{x^4 + \Lambda^4}.$$

Similarly we can write $\bar{I}_2 = \bar{I}_{21} + \bar{I}_{22}$ with

$$\bar{I}_{21} = \frac{1}{i\pi}\int_{-\infty}^{-\mu} dy \frac{(y+\mu)^3}{y-z} \frac{\Lambda^4}{(y+\mu)^4 + \Lambda^4} \psi\left(\frac{1}{2} - \frac{i\beta y}{2\pi}\right) = \frac{1}{i\pi}\left\{2\pi i \frac{\left(\Lambda e^{\frac{3\pi i}{4}}\right)^3}{\Lambda e^{\frac{3\pi i}{4}} - (z+\mu)}\right.$$
$$\left.\times \frac{\Lambda \psi\left(\frac{1}{2} + i\frac{\beta\mu}{2\pi} - i\frac{\beta\Lambda}{2\pi}e^{\frac{3\pi i}{4}}\right)}{\left(e^{\frac{3\pi i}{4}} - e^{\frac{\pi i}{4}}\right)\left(e^{\frac{3\pi i}{4}} - e^{\frac{-\pi i}{4}}\right)\left(e^{\frac{3\pi i}{4}} - e^{\frac{-3\pi i}{4}}\right)} - \int_0^{\infty} dx \frac{x^3}{ix - (z+\mu)}\left[\frac{\Lambda^4 \psi\left(\frac{1}{2} + i\frac{\beta\mu}{2\pi} + \frac{\beta x}{2\pi}\right)}{x^4 + \Lambda^4}\right]\right\}$$

and

$$\bar{I}_{22} = \frac{-1}{i\pi}\int_{-\mu}^{\infty} dy \frac{(y+\mu)^3}{y-z} \frac{\Lambda^4}{(y+\mu)^4 + \Lambda^4} \psi\left(\frac{1}{2} - \frac{i\beta y}{2\pi}\right) = \frac{1}{i\pi}\left\{2\pi i \frac{\left(\Lambda e^{\frac{\pi i}{4}}\right)^3}{\Lambda e^{\frac{\pi i}{4}} - (z+\mu)}\right.$$
$$\times \frac{\Lambda \psi\left(\frac{1}{2} + i\frac{\beta\mu}{2\pi} - i\frac{\beta\Lambda}{2\pi}e^{\frac{\pi i}{4}}\right)}{\left(e^{\frac{\pi i}{4}} - e^{\frac{-\pi i}{4}}\right)\left(e^{\frac{\pi i}{4}} - e^{\frac{3\pi i}{4}}\right)\left(e^{\frac{\pi i}{4}} - e^{\frac{-3\pi i}{4}}\right)} + 2\pi i \frac{(\mu+z)^3\Lambda^4}{(\mu+z)^4 + \Lambda^4} \psi\left(\frac{1}{2} - i\frac{\beta z}{2\pi}\right)$$
$$\left. - \int_{\infty}^{0} dx \frac{x^3}{ix - (z+\mu)}\left[\frac{\Lambda^4 \psi\left(\frac{1}{2} + i\frac{\beta\mu}{2\pi} + \frac{\beta x}{2\pi}\right)}{x^4 + \Lambda^4}\right]\right\}.$$

Thus

$$\bar{I}_2 = \bar{I}_{21} + \bar{I}_{22} = \frac{\Lambda^4 \psi\left(\frac{1}{2} + i\frac{\beta\mu}{2\pi} - i\frac{\beta\Lambda}{2\pi}e^{\frac{3\pi i}{4}}\right)}{2\left(\Lambda e^{\frac{3\pi i}{4}} - (z+\mu)\right)} - \frac{\Lambda^4 \psi\left(\frac{1}{2} + i\frac{\beta\mu}{2\pi} - i\frac{\beta\Lambda}{2\pi}e^{\frac{\pi i}{4}}\right)}{2\left(\Lambda e^{\frac{\pi i}{4}} - (z+\mu)\right)} - 2\frac{(z+\mu)^3\Lambda^4}{(z+\mu)^4 + \Lambda^4} \psi\left(\frac{1}{2} - i\frac{\beta z}{2\pi}\right)$$
$$-\frac{2}{i\pi}\int_0^{\infty} dx \frac{x^3}{ix - (z+\mu)}\left[\frac{\Lambda^4 \psi\left(\frac{1}{2} + i\frac{\beta\mu}{2\pi} + \frac{\beta x}{2\pi}\right)}{x^4 + \Lambda^4}\right].$$

We combine results of $\bar{I}_1$ and $\bar{I}_2$ to get

$$R_{\mathrm{SP}}(z) = \frac{4}{9\pi t^4}(\bar{I}_1 + \bar{I}_2) = \frac{16}{81\pi t^4}\left\{\frac{2\Lambda^4}{\pi}\int_0^{\infty} dx \frac{x^3}{x^4 + \Lambda^4} F(x,\mu,z) - 2\frac{(z+\mu)^3\Lambda^4}{(z+\mu)^4 + \Lambda^4} \psi\left(\frac{1}{2} - i\frac{\beta z}{2\pi}\right)\right.$$
$$\left. + \mathrm{Re}\left[\frac{\Lambda^4 \psi\left(\frac{1}{2} + i\frac{\beta\mu}{2\pi} - i\frac{\beta\Lambda}{2\pi}e^{\frac{3\pi i}{4}}\right)}{\Lambda e^{\frac{3\pi i}{4}} - (z+\mu)} - \frac{\Lambda^4 \psi\left(\frac{1}{2} + i\frac{\beta\mu}{2\pi} - i\frac{\beta\Lambda}{2\pi}e^{\frac{\pi i}{4}}\right)}{\Lambda e^{\frac{\pi i}{4}} - (z+\mu)}\right]\right\}.$$

[1] J. H. Chen, W. G. Cullen, E. D. Williams, and M. S. Fuhrer, Nature Physics, advanced online publication (2011), doi: 10.1038/nphys1962.

[2] P. O. Lehtinen, A. S. Foster, Y. Ma, A. V. Krasheninnikov, and R. M. Nieminen, Phys. Rev. Lett. **93**, 187202 (2004).

[3] O. V. Yazyev, Phys. Rev. Lett. **101**, 037203 (2008).

[4] P. Esquinazi, D. Spemann, R. Hohne, A. Setzer, K.-H. Han, and T. Butz, Phys. Rev. Lett. **91**, 227201 (2003).

[5] M. M. Ugeda, I. Brihuega, F. Guinea, and J. M. Gomez-Rodriguez, Phys. Rev. Lett. **104**, 096804 (2010).

[6] J. J. Palacios, J. Fernandez-Rossier, and L. Brey, Phys. Rev. B **77**, 195428 (2008).

[7] B. Uchoa, T. G. Rappoport, and A. H. Castro Neto, Phys. Rev. Lett. **106**, 016801 (2011).

[8] B. Uchoa, V. N. Kotov, N. M. R. Peres, and A. H. Castro Neto, Phys. Rev. Lett. **101**, 026805 (2008).

[9] J. R. Schrieffer and P. A. Wolff, Phys. Rev. **149**, 491 (1966).

[10] K. H. Fischer, Z. Phys. B **42**, 27 (1981).

[11] Y. Nagaoka, Phys. Rev. **138**, A1112 (1965).

[12] H. Suhl, Phys. Rev. **138**, A515 (1965).

[13] D. Withoff and E. Fradkin, Phys. Rev. Lett. **64**, 1835 (1990).

[14] K. Ingersent, Phys. Rev. B **54**, 11936 (1996).

[15] C. Gonzalez-Buxton and K. Ingersent, Phys. Rev. B **54**, R15614 (1996).

[16] A. Polkovnikov, Phys. Rev. B **65**, 064503 (2002).

[17] K. Sengupta and G. Baskaran, Phys. Rev. B **77**, 045417 (2008).

[18] M. Vojta and R. Bulla, Phys. Rev. B **65**, 014511 (2001).

[19]M. Vojta, L. Fritz, and R. Bulla, Europhys. Lett. **90**, 27006 (2010).
[20]L. Fritz and M. Vojta, Phys. Rev. B **70**, 214427 (2004).
[21]L. Brey, H. A. Fertig, and S. Das Sarma, Phys. Rev. Lett. **99**, 116802 (2007).
[22]S. Saremi, Phys. Rev. B **76**, 184430 (2007).
[23]P. W. Anderson, Phys. Rev. **124**, 41 (1961).
[24]T. A. Costi, A. C. Hewson, and V. Zlatic, J. Phys. Condens. Matter **6**, 2519 (1994).
[25]A. C. Hewson, *The Kondo Problem to Heavy Fermions*, Cambridge Studies in Magnetism (Cambridge University Press, Cambridge, UK, 1993).
[26]P. B. Wiegman and A. M. Tsvelik, J. Phys. C **16**, 2281 (1983); Adv. Phys. **32**, 453 (1983).